https://doi.org/10.5194/egusphere-2026-623
Preprint. Discussion started: 5 March 2026

Sequential approach to seismotectonic zonation for South-East France

Victoria Mowbray[1], Marguerite Mathey[2], Christian Sue[1], Stéphane Baize[2], Anne Lemoine[3], Céline Beauval[1]

[1]Institut Sciences de la Terre, UGA, USMB, CNRS, IRD, OSUG, Gières, France
[2]Autorité de Sûreté Nucléaire et de Radioprotection, Fontenay-aux-Roses, France
[3]Bureau de Recherches Géologiques et Minières, Orléans, France

Correspondence to: Victoria Mowbray (victoria.mowbray@univ-grenoble-alpes.fr)

Abstract. The south-east of France, encompassing the western Alps, the Jura Mountain range, the Rhône valley and the Provence region, is the most seismically active region in metropolitan France and, consequently, one of the most extensively surveyed and studied. However, seismicity remains low to moderate (less than 10 Mw 5 and 1 Mw 6 events per century since 1300 CE) and geodetic deformation rates appear relatively low (< 20 nanostrain yr^{-1}). The resulting low-signal-to-noise ratios, together with the complex, dense fault networks inherited from a polyphased tectonic history, make this region particularly challenging for seismic hazard assessment. The geophysical and geological data available are extensive, yet inhomogeneous and insufficient to confidently characterize active faults, quantify on-fault deformation and associate seismic rates. Therefore, seismic source characterization through seismogenic area models is commonly adopted. These models are however highly sensitive to the data used to describe seismotectonic behavior. Our objective is to consider newly available geophysical data as complementary constraints to geological observations to further refine seismotectonic zonation models.

We present an innovative sequenced zoning methodology that disaggregates seismotectonic behavior into three components (namely – crustal structure, observed seismicity and surface deformation) each analyzing several key features. We thus derive three novel, independent seismotectonic zonation models, each representing a different perspective on the seismogenic process. Additionally, we associate confidence levels with zone limits to each subsequent zonation model, by assessing feature homogeneity among neighboring zones. Afterwards, we propose a synthetic model which integrates all seismotectonic features by merging the most recurrent and highest confidence zone limits from the three independent zonation models. This approach intends to minimize zone mapping uncertainties by quantitatively assessing seismotectonic observations, and to yield reproducible and updatable models representative of the current state of seismotectonic knowledge. We subsequently compare the resulting zonation models and discuss their implications for seismic source characterization.

1 Introduction

The south-east of mainland France presents low to moderate seismicity (e.g. Larroque et al., 2021) and slow crustal deformation, within the 0 – 20 nanostrain yr^{-1} range (Walpersdorf et al., 2018; Masson et al., 2019; Serpelloni et al., 2022). Nevertheless, 27 Mw ≥ 5.5 events, and 7 Mw ≥ 6 are documented since 1356 CE. (FCAT, 463 – 1961, Manchuel et al., 2018; BCSF Rénass, 1962 – 2021, BCSF-Rénass, 2022; ESHM20 Unified Earthquake catalog, 1000 – 2014, Danciu et al., 2024) in the area (Fig. 1), pointing to a significant activity in terms of natural hazard. The polyphased tectonic history that South-East France has experienced (e.g. Malavieille, 1993; Le Pichon and Rangin, 2010; Mohn et al., 2012; Bellahsen et al., 2014; Boschetti et al., 2025) and the resulting complex geological structure make this region tectonically, and thus seismically, heterogeneous. The present-day geodynamics and seismotectonic framework are a complex and active topic of debate (e.g. Sternai et al., 2019; Mathey et al., 2021; Grosset et al., 2023), contrasted among the high Alpine belt -extension and trans-tension- and its peripheral basins -strike-slip and trans-pression- (e.g., Sue et al., 1999, 2007a; Delacou et al., 2004, 2005; Mathey et al., 2021) confirmed by GNSS surveys (Walpersdorf et al., 2015, 2018).

This framework, alongside the uneven distribution of geophysical monitoring efforts (Jenatton et al., 2007; Walpersdorf et al., 2015; Mathey et al., 2020; Guéguen et al., 2022; Langlais et al., 2024), is insufficient to confidently identify all active faults and determine associated seismic rates, in comparison to more seismically

https://doi.org/10.5194/egusphere-2026-623
Preprint. Discussion started: 5 March 2026

active contexts. In addition, erosion rates exceed tectonic rates (Sternai et al., 2019; Valla et al., 2021), challenging the characterization of long-recurrence seismic patterns at the surface. Consequently, fault-based models for Seismic Hazard Assessment (SHA) are strongly affected by uncertainties in such a low to moderate seismicity region. For this reason, in such seismotectonic framework, zonation models are often employed to forecast diffuse seismicity (e.g. Coppersmith et al., 2009; Woessner et al., 2015; Martin et al., 2018; Danciu et al., 2021), such is the case for mainland France. Seismotectonic Zonation Models (SZM) define data-driven zones assumed to be homogeneous in terms of seismogenic behavior and potential, and may thus be used in seismic hazard assessments, for example, to define earthquake rates, seismogenic depth, maximum expected magnitudes and the deformation mode.

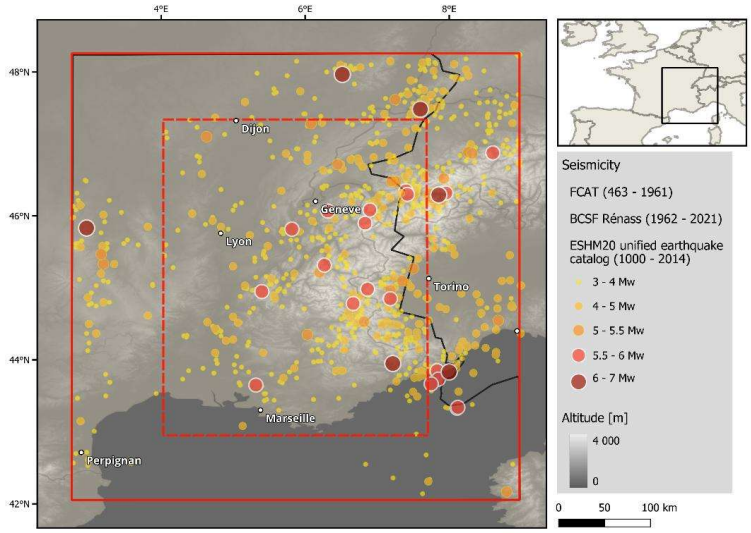

Figure 1: Definition of the study area, with the targeted south-east of France (dashed red rectangle). We expand the data sample to a larger area encompassing 100 km over its boundaries (solid red rectangle) in order to account for seismic sources susceptible of causing hazard in the target area. Seismicity from the FCAT (463 – 1961; Manchuel et al., 2018) and BCSF Rénass (1962 – 2021; BCSF-Rénass, 2022) catalogs for metropolitan France, and ESHM20 Unified Earthquake catalogue (1000 – 2014; Danciu et al., 2024), for the off-boundary regions. The catalog junction limit is expressed with a black line. Digital elevation model obtained from Hengl et al. (2022).

The current regulatory seismic zoning in France, used in building codes, is based on seismic hazard maps obtained from applying the Probabilistic Seismic Hazard Assessment (PSHA) method (seminal articles by Cornell, 1968; McGuire, 1976; hazard calculations for France by Martin et al., 2002). These hazard calculations produced over 20 years from now used the seismotectonic zones from the EPAS model (Autran et al., 1998). Several SZM for France have been produced since, both by the private sector and by state operators (Terrier et al., 2000; Martin et al., 2002; Baize et al., 2013; Le Dortz et al., 2019). They assess and incorporate mainly structural, seismotectonic, and seismic data. Hence, other geophysical data, such as geodetic observations, have not been widely exploited in this purpose previously.

The objective of this work is to update and improve the seismic source characterization for PSHA of South-East France through seismotectonic zone modeling. For this we analyze seismotectonic observations for a large area encompassing 100 km from the region of interest (solid rectangle in Fig. 1) based on the inventory of available data: geological maps, 3D geological models, fault databases, seismic tomography studies, seismic records, focal mechanism solutions, GNSS strain-rate and velocity solutions, and InSAR vertical displacement solutions. As a result, we develop and present three independent SZM based on distinct observable classes: a crustal structure-based model, a seismicity-based model, and a deformation-based model; each offering a distinct, complementary, insight on seismic hazard. The structure-based SZM informs on the geological environment hosting the seismicity, the seismicity-based SZM reflects the spatial distribution of released seismic energy, while the deformation-based SZM captures the crustal deformation inferred from geodetical surface measurements.

https://doi.org/10.5194/egusphere-2026-623
Preprint. Discussion started: 5 March 2026

As an attempt to assess uncertainties linked to zone mapping, we propose an innovative approach to evaluate zone boundaries. Hierarchization of zone boundaries is recurrently applied (e.g. Autran et al., 1998; Baize et al., 2013; Le Dortz et al., 2019), as it allows propagation of zone delineation uncertainties and permits grouping certain areas with the purpose of increasing the seismic sample to be considered in earthquake recurrence estimates. In this line, we quantitatively estimate the feature heterogeneity among neighboring zones and correspondingly give levels of confidence to each zone limit.

Finally, we combine the highest confidence zone limits from the three independent SZM to construct a synthetic fourth zonation model, named "unified model", which accounts for all the seismotectonic features we considered. The four resulting models may be used as alternative models in a future PSHA study for southeastern France. We thus compare the zonation models with one another as well as with existing ones and discuss their added value and limitations for improving seismic source characterization.

2 Seismotectonic Zonation Model Methodology

We build three Seismotectonic Zonation Models (SZM), allowing the characterization of seismic source through different processes and time spans: the occurrence of earthquakes in a given geological context informing on long-term processes, seismic energy release viewed through earthquake catalogs, and energy accumulation in the crust viewed by geodesy; giving place to a structural-based SZM, a seismicity-based SZM and a deformation-based SZM, respectively.

In the following approach, each of these models incorporates three key seismotectonic features (hereafter F1, F2, F3), which may be defined by one or various complementary observables (Table 1). For each observable, we inventory, analyze and discretize up-to-date, relevant data. We then delineate polygons which englobe areas with similar data values, for each subsequent model, by identifying spatial distribution patterns.

The structural model delineates areas with near-homogeneous crustal structure. It is constructed from geology (maps and 3D models), faults (a fault data compilation and a fault model for SHA), and crustal thickness (tomographic studies). The seismicity model quantifies the seismic energy released through seismic observables - seismic flux evaluated using both instrumental (~60 yr) and historical (~700 yr) records, rupture mode obtained from focal mechanisms (~60 yr) and seismogenic depth analyzed using various instrumental catalogs (~60 yr). The deformation model reflects strain accumulation by analyzing crustal deformation (horizontal deformation amplitude and mode, and vertical displacement) inferred from geodetic interpretations (GNSS acquisitions ~25 yr, InSAR acquisitions ~5 yr).

To enhance the robustness of our zoning approach, we chose to quantify data heterogeneity among zones, thereby allowing for an objective assessment of zone limit delineation. We compute for each of the three models, the average value of each feature per zone, giving contribution weights for each considered dataset (Table 1). We then evaluate the difference for the three key features among neighboring zones in order to attribute confidence levels to zone limits (CLZL). These levels reflect high confidence when the combination of differences is high, intermediate confidence when it's average, and low when the differences are small.

SZM	Feature		Observable	Dataset	Contribution weight
Structure-based	F1	Geology	Surface chronostratigraphy units	Geological map	Qualitative analysis
			Basin cover thickness	3D Geological models	
	F2	Faults	Mean azimuth	SEFPAF fault database	
			Amount of fracture		
			Seismogenic potential index		
			Main fault from fault source model		
	F3	Crustal thickness	Moho depth	Seismic tomography model	
Seismicity-based	F1	Seismic flux	Mean annual seismic moment per area	FCAT – BCSF catalogs	0.8
				ESHM20 catalog	0.2

https://doi.org/10.5194/egusphere-2026-623
Preprint. Discussion started: 5 March 2026

	F2	Rupture mechanism	Style of faulting from the moment tensor of an area	Focal mechanism databases	1
	F3	Seismogenic depth	D90 quantile for areas of events > 10	SISMALP catalog	0.5
				BCSF Rénass catalog	0.1
				ISIDe catalog	0.4
Deformation-based	F1	Horizontal deformation amplitude	Maximum GNSS derived strain-rate	GNSS strain-rate solution 1	0.8
				GNSS strain-rate solution 2	0.2
	F2	Horizontal deformation style	Deformation mode after GNSS derived strain-rate tensors	GNSS strain-rate solution 1	0.8
				GNSS strain-rate solution 2	0.2
	F3	Vertical displacement	GNSS and InSAR derived vertical velocity	GNSS velocity solution 1	0.5
				GNSS velocity solution 2	0.5
				InSAR solution	Qua an

Table 1: Logigram of the features, observables, datasets and contribution weights applied for each of the three seismotectonic zonation models. See *Data analysis* for further dataset information.

3 Data analysis

3.1 Structure-based Seismotectonic Zonation Model

The structural SZM (St-SZM) is based on the following three key features: geology (F1), faults (F2) and crustal thickness (F3).

F1: Geology

The rheology, thickness and superposition of diverse geological units may affect the seismogenic potential of the crust (Chiaraluce et al., 2017, Petit et al., 2019). For this reason, we distinguish two observables that characterize this feature: surface stratigraphy and basin cover thickness.

To assess surface geology we focus on distinguishing the main chronostratigraphic horizons given by the geological map of France (Chantraine et al., 2003), differentiating Cenozoic, Mesozoic and Paleozoic-Proterozoic units (Fig. 2a). In order to include the depth dimension, we integrate 3D geological models (GeoMol Project Team., 2019; Bienveignant et al., 2024) for the Swiss Molasse basin and the Rhône valley. From these, we distinguish the limit between the Cenozoic and Mesozoic from crystalline basement units, thus informing on the thickness of the sedimentary crustal units composing the basin cover (Fig. 2b).

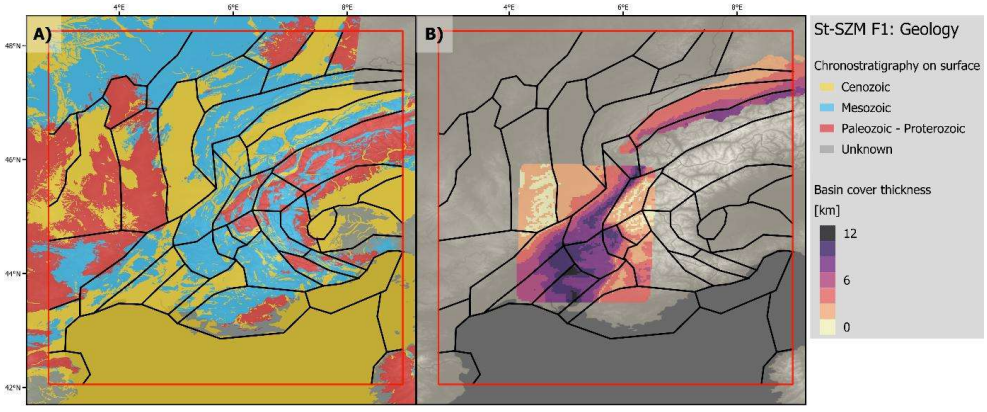

Figure 2: Geological data used to characterize F1 (geology) of the structure-based SZM. A) Geological map showing the surface stratigraphy grouping units by geological Eras (modified from Chantraine et al., 2003); B) Thickness of basin

https://doi.org/10.5194/egusphere-2026-623
Preprint. Discussion started: 5 March 2026

cover units (Cenozoic and Mesozoic) available for the Rhone valley (Bienveignant et al., 2024) and the Swiss Molasse basin (GeoMol Project Team, 2019). Both A) and B) are superposed with the resulting zone limits of the St-SZM.

F2: Faults

In order to integrate the current state of knowledge on faults as locus where future earthquakes may occur, we take into account the following observables: fault azimuth tendency, amount of fracture per region, estimated seismogenic potential and main faults considered for a fault-based seismic source model. We define homogenous ensembles assessing these four observables from the structural standpoint using SEFPAF database (South-East France Potentially Active Faults, Mowbray et al., 2025, Fig. 3a) and its associated selection of faults for a fault-based source model (Fig. 3b). The latter presents idealized fault geometries, giving place to composite seismogenic sources (Basili et al., 2008).

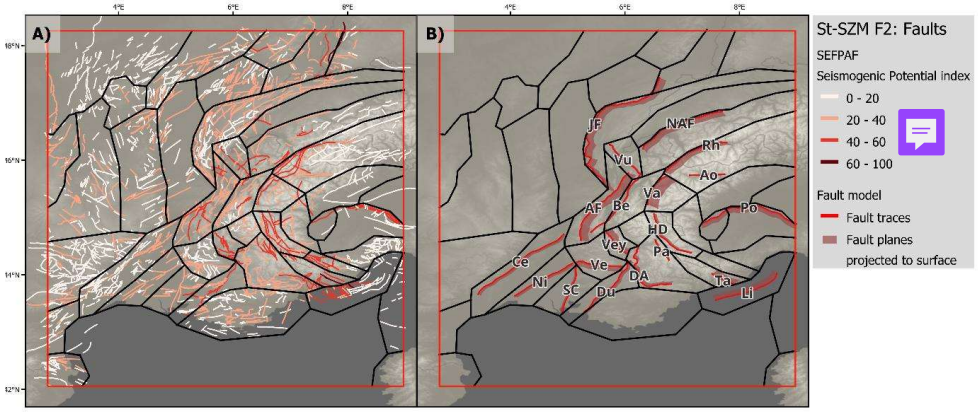

Figure 3: Fault data considered to characterize F2 (faults) of the structure-based SZM. A) Fault traces and their seismogenic potential index from SEFPAF (South East France Potentially Active Faults, Mowbray et al., 2025); B) Selected faults for a fault-based source model for SHA (Mowbray et al., 2025). Fault acronyms: JF: Jura-Front, NAF: North-Alpine-Front, Vu: Vuache, Rh: Rhone, Ao: Aosta, Po: Po, Li: Ligure, Ta: Taggia, Pa: Parpaillon, HD: High-Durance, Va: Valloire, Be: Belledonne, AF: Alpine-Front, Vey: Veynes, Ve: Ventoux, DA: Digne-Arc, Du: Durance, SC: Salon-Cavaillon, Ni: Nimes, Ce: Cevennes. Both A) and B) are superposed with the resulting zone limits of the St-SZM.

F3: Crustal thickness

Crustal thickness may provide insight on maximum expected depth for large earthquakes (Spooner et al., 2019). To characterize this feature we use a Moho depth proxy from a recent seismic tomography study (Nouibat et al., 2022 after Nouibat 2024, using the isovelocity 4.2 km s^{-1}) and a digital elevation model of continental Europe (Hengl et al., 2022) in order to obtain the crust thickness (Fig. 4). This tomographic study is generally in agreement with other recent studies of the Alpine Moho depth (Lu et al., 2018, Braszus et al., 2025). However, the isovelocity criterion differs between Moho domains - the Adriatic Moho along the Ivrea mantle body (see Fig. C1 for geographical reference) requires a Vs = 3.8 km s^{-1} while the European Moho, a Vs = 4.2 km s^{-1} -, therefore, a fully

https://doi.org/10.5194/egusphere-2026-623
Preprint. Discussion started: 5 March 2026

three-dimensional model on the crust-mantle boundary along the Alpine range would ideally be required.

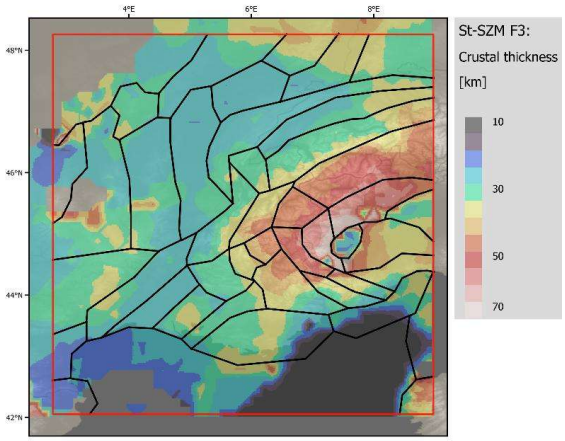

Figure 4: F3 (crustal thickness) of the structure-based SZM inferred from seismic tomography (Nouibat, 2024, computed at Vs = 4.2 km s^{-1}) and a digital elevation model (Hengl et al., 2022). The figure is superposed with the resulting zone limits of the St-SZM.

3.2 Seismicity-based Seismotectonic Zonation Model

Based on available earthquake and focal mechanism catalogs, the seismicity SZM (Se-SZM) considers the 3 following features: seismic flux (F1), rupture mechanism (F2) and seismogenic depth (F3). We examine seismic events using two grids with hexagonal cells of about 11 km and 55 km (0.1° and 0.5° in EPSG:4326 - WGS 84, respectively) of diameter, allowing us to decipher data patterns at both fine and coarse scale, and account for the heterogeneous location uncertainties of instrumental and historical data.

F1: Seismic flux

Events with magnitude above 3 dominate the total seismic flux. For this reason, we use seismic catalogs with long temporal coverage. Within France we use FCAT (Manchuel et al., 2018) for the historical period (463 – 1962), combined with the BCSF-Rénass catalog (BCSF-Rénass, 2022) for the instrumental period (1962 – 2021; Fig. 5a). The data from these records extend 40 km beyond national borders for the historical events, and 20 km for the instrumental. To cover the areas outside of the French territory we complement with the ESHM20 Unified Earthquake catalog (1000 – 2014; Danciu et al., 2024; Fig. 5b), which itself is a combination of the European historical catalog EPICA (Rovida et al., 2022) and the instrumental European catalog EMEC (Lammers et al., 2023).

Seismic moment rates are estimated for the events in these catalogs falling within the considered completeness periods (Fig. A1, A2, Table 2), setting a minimum magnitude threshold of Mw 2 for FCAT and BCSF – Rénass, and Mw 3.5 for ESHM20. To do so we compute the seismic moment per event from its magnitude (Hanks and Kanamori, 1979), and divide it by the time period of completeness for the given magnitude. Finally, we sum the event rates within each grid cell and divide it by the cell area. We classify seismic flux values in four bins representative of the data set: $10^{6} – 10^{9}$, $10^{9} – 10^{11}$, $10^{11} – 10^{13}$, $10^{13} – 10^{16}$ (N m yr^{-1} km^{-2}) (Fig. 5c-5f); allowing for a better identification of spatial seismic energy release patterns.

Magnitude interval	2 – 2.5	2.5 – 3	3 – 3.5	3.5 – 4	4 – 4.5	4.5 – 5	5 – 5.5	5.5 – 6	6 – 6.5	6.5 – 7
Completeness periods FCAT + BCSF Rénass	1975 – 2021	1960 – 2021	1840 – 2021	1830 – 2021	1810 – 2021	1810 – 2021	1775 – 2021	1750 – 2021	1475 – 2021	1350 – 2021
Completeness periods ESHM20				1860 – 2014	1850 – 2014	1810 - 2014	1750 – 2014	1750 – 2014	1350 – 2014	1350 – 2014

Table 2: Estimation of completeness time periods per 0.5 magnitude interval (Mw) for FCAT (Manchuel et al., 2018) + BCSF Rénass (BCSF-Rénass, 2022) and ESHM20 catalogs (Danciu et al., 2024). Considering events falling within the area of interest (solid red rectangle in Figure 1).

https://doi.org/10.5194/egusphere-2026-623
Preprint. Discussion started: 5 March 2026

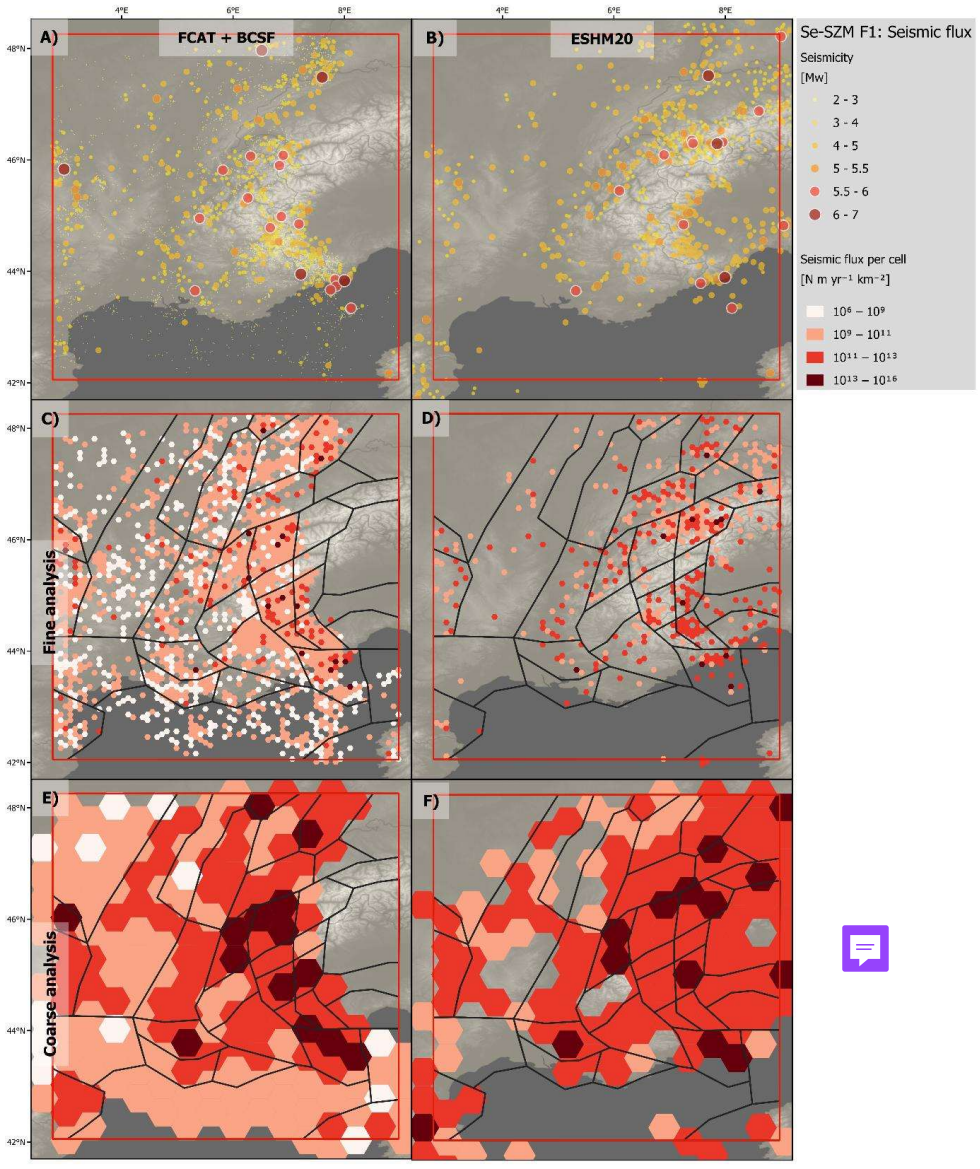

Figure 5: Seismic data used to characterize F1 (seismic flux) of the seismicity-based SZM. A, B) Seismic records showing events falling within each catalog completeness range: A) FCAT (1356 – 1961) + BCSF Rénass (1962 – 2021), Mw > 2; B) ESHM20 Unified catalog (1356 - 2014), Mw > 3.5; C), D) seismic flux computed on A) and B) respectively, within the fine grid; E), F) seismic flux computed on A) and B) respectively, within the coarse grid; C) to F) are superposed with the resulting zone limits of the Se-SZM.

F2: Rupture mechanism

The mode of crustal deformation expressed seismically - normal, reverse, strike-slip or oblique - is inferred from focal mechanisms. These provide direct information on recorded earthquake ruptures, thus informing on crustal stress released seismically at depth.

https://doi.org/10.5194/egusphere-2026-623
Preprint. Discussion started: 5 March 2026

We use the focal mechanisms from Mathey et al. (2021), (1989 – 2015) for the Alpine range itself and complement it with the FMHex catalog (1954 - 2024, plus one event in 1909, Mazzotti et al., 2021) for events located in the surrounding regions (Fig. 6a shows only events of Mw > 3 for visualization purposes). We use moment magnitude, dip, rake and strike values to compute the summed seismic moment tensor using the Kostrov (1974) approach (see also Sue et al., 2007b). We subsequently derive the eigenvalues of the strain-rate tensor and the T, P, and B axes representative of each grid cell. We thus determine the faulting style for each cell using the Fröhlich (1992) classification for both fine and coarse grids (Fig. 6b, 6c).

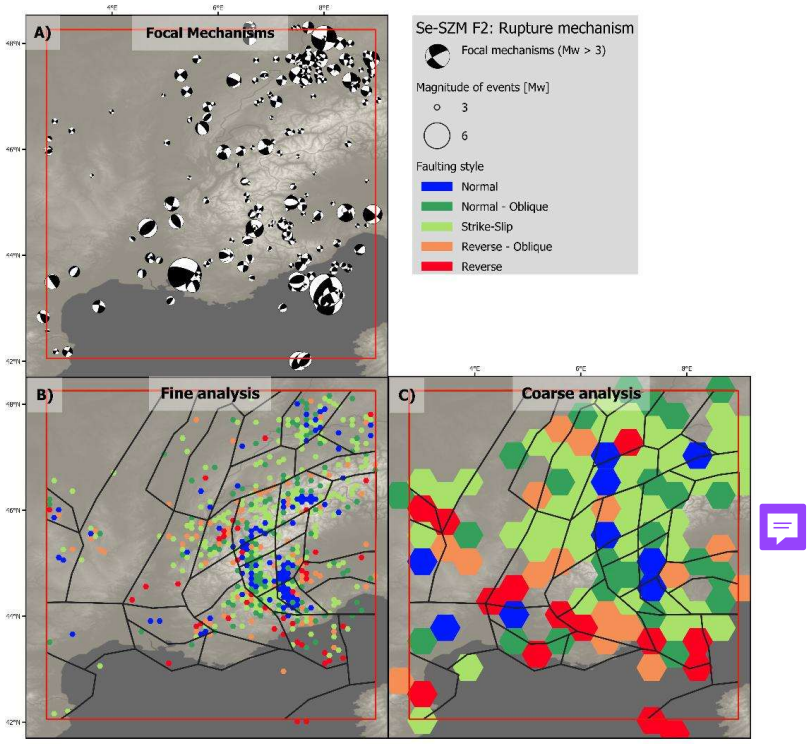

Figure 6: Seismotectonic data used to characterize F2 (rupture mechanism) of the seismicity-based SZM. A) Focal mechanisms for events with Mw > 3 from Mathey et al., 2021 (1962 – 2013) and Mazzotti et al., 2021 (1962 – 2019); B), C) Faulting style deduced from T, P and B, axes obtained with computed moment tensors for all magnitude events within cells of both fine and coarse grids, respectively. Both B) and C) are superposed with the resulting zone limits of the Se-SZM.

F3: Seismogenic depth

The seismogenic depth is conditioned by crustal rheology, geodynamic processes and the location of structures accommodating the deformation (Zielke et al., 2020). We obtain this value from the distribution of hypocenter depths. A good resolution of hypocenter location is required, thus only instrumental catalogs are used. We consider grid cells containing at least 10 earthquakes, and compute the 90% depth quantile (D90) for the cell. We distinguish five seismogenic depth levels which allow to identify patterns for this feature and are representative of the uncertainty range for hypocenter location; < 5, 5 – 10, 10 – 15, 15 – 20 and > 20 (km).

We consider all events in the instrumental catalogs SISMALP (1987 – 2024; Langlais et al., 2024), BCSF-Rénass (1962 – 2021; BCSF-Rénass, 2022) and ISIDe (1985 – 2023; ISIDe Working Group, 2007) to constrain the D90, for both sizes of grid cells (Fig. 7). However, the temporal extension of the three catalogs and the depth uncertainties differs, affecting the density of events at depth and consequently the D90.

https://doi.org/10.5194/egusphere-2026-623
Preprint. Discussion started: 5 March 2026

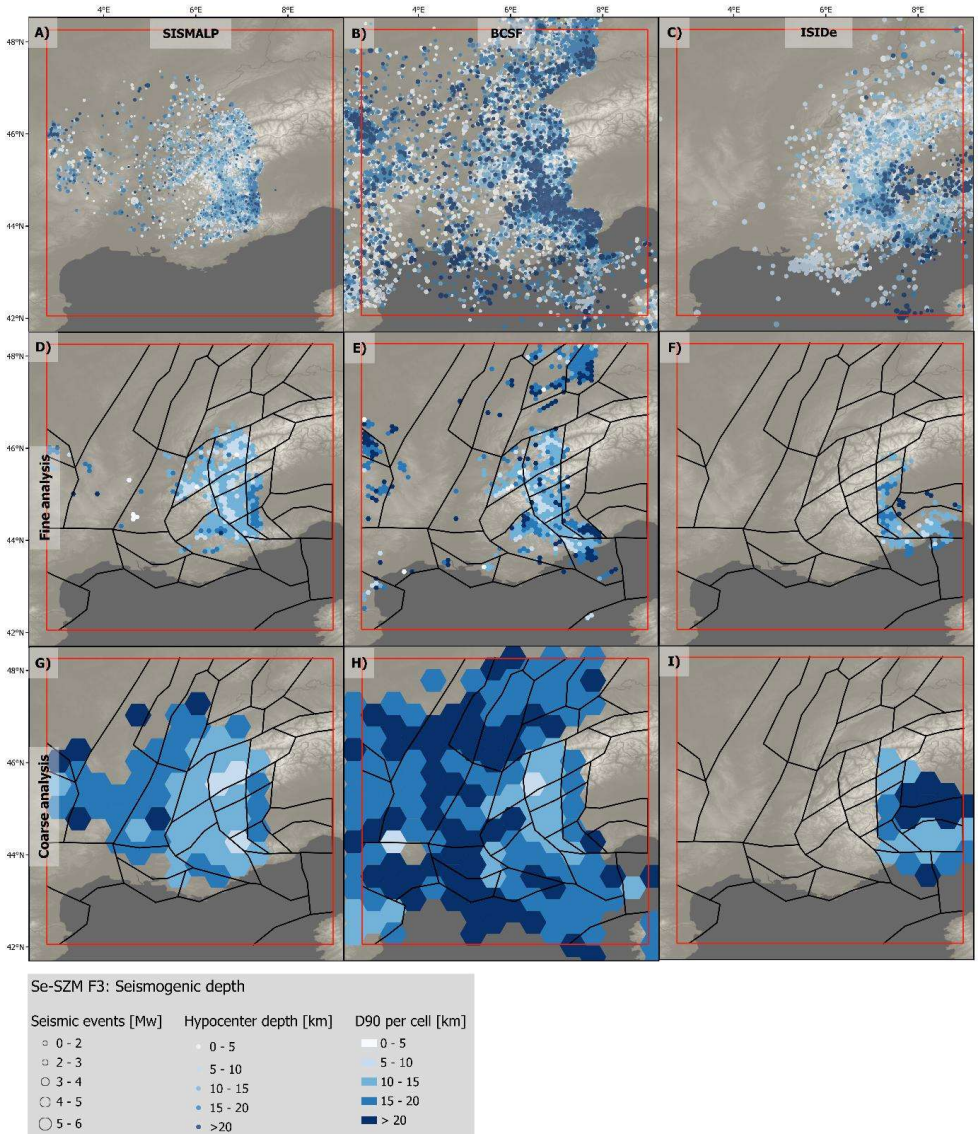

Figure 7: Seismic data used to characterize F3 (seismogenic depth) of the seismicity-based SZM. A), B), C) Hypocentral depths and moment magnitude of the seismic events from SISMALP (1987 – 2024), BCSF-Rénass (1962 – 2021) and ISIDe (1985 – 2023), respectively; D), E), F) Seismogenic depths computed as D90 within cells of the fine grid (presenting > 10 events), for the three catalogs respectively; G), H), I) Seismogenic depth computed as D90 within cells of the coarse grid (presenting > 10 events), for the three catalogs respectively; D) to I) are superposed with the resulting zone limits of the Se-SZM.

3.3 Deformation-based Seismotectonic Zonation Model

We attempt, in the deformation SZM (De-SZM), to consider the geodetically inferred surface deformation measured by GNSS and InSAR. The leading hypothesis is that part of this interseismic deformation can be released seismically. Therefore, geodesy may inform on where seismic stress is being accumulated, and ultimately, on a potential location for future earthquakes. It thus appears relevant to consider geodetic data to define homogeneous

https://doi.org/10.5194/egusphere-2026-623
Preprint. Discussion started: 5 March 2026

areas in terms of crustal deformation amplitude and mode. However, the short time-span of GNSS measurements (< 25 years) along with the high uncertainties related to low deformation contexts result in GNSS solutions showing major discrepancies.

GNSS vertical velocity uncertainties are notably higher than horizontal ones (Masson et al., 2019; Serpelloni et al., 2022). We aim to account for these uncertainties by complementing GNSS data with velocities derived from InSAR (Mathey et al., 2022). Moreover, vertical movements at large-scale are a product of multiple geodynamic processes not intrinsically accommodated in the brittle crust (e.g. glacial and gravitational isostasy, dynamic topography, and mantle buoyancy), therefore, its relation with seismicity is not yet comprehensively understood (Sternai et al., 2019; Piña-Valdés et al., 2022).

Hence, we assess geodetic deformation considering separately horizontal strain-rates and vertical displacement. The features analyzed in this model are horizontal deformation amplitude (F1), horizontal deformation mode (F2) and vertical displacement (F3). As in the previous model, the data is represented in hexagonal grid cells, applying the fine or coarse grid (hexagonal grid cell diameters of 0.1° and 0.5° in EPSG:4326 - WGS 84, respectively) depending on the density and resolution of each dataset.

F1: Horizontal deformation amplitude

To evaluate horizontal strain-rate spatial variation, we examine two different GNSS strain-rate solutions (GNSS s1: Piña-Valdés et al., 2022; GNSS s2: Lantmäteriet, 2023; Fig. 8a, 8b). The first solution uses an interpolation method that captures small wave-length, large amplitude strain variations, but may also accentuate artefacts. The latter employs a smoother, lower-resolution interpolation method, revealing coarser spatial variations yet smaller strain values, as high strain peaks are attenuated. These contrasting results reflect the impact of methodological choices. To best represent each solution, we map the strain-rate amplitude in the small and large cell grids, respectively for the high and low-resolution datasets. To compare both solutions we use the amplitude of deformation (E) from the eigenvalues of the strain-rate tensor (Eq. 1; Masson et al., 2019):

$$E = \max(|emin|, |emax|, |emin+emax|) \quad (1)$$

Where emax and emin are the maximum and minimum principal strain-rate axes. We chose to categorize strain-rate amplitude in bins representative of the dataset, and allowing pattern identification: $< 3, 3-5, 5-7, 7-9, > 9$ (nanostrain yr^{-1}) (Fig. 8c, 8d).

F2: Horizontal deformation mode

We represent the geodetic horizontal mode of deformation using the same two GNSS strain-rate solutions (GNSS s1: Piña-Valdés et al., 2022; GNSS s2: Lantmäteriet, 2023), classifying deformation modes (M) from normalized principal strains rates (Eq. 2; Jeandet et al., submitted):

$$M = (emax + emin)/E \quad (2)$$

Where emax and emin are the maximum and minimum principal strain-rate axes and E is the strain-rate amplitude. Thus M = -1 represents compression, M = 0, strike-slip, and M = 1, extension (Fig. 8e, 8f). The differing solutions lead to variations in the deformation mode, particularly in areas of low strain, where artefact influence can dominate. For this reason, we consider only cells with strain-rate amplitudes higher or equal to 3 nanostrain yr^{-1}.

https://doi.org/10.5194/egusphere-2026-623
Preprint. Discussion started: 5 March 2026

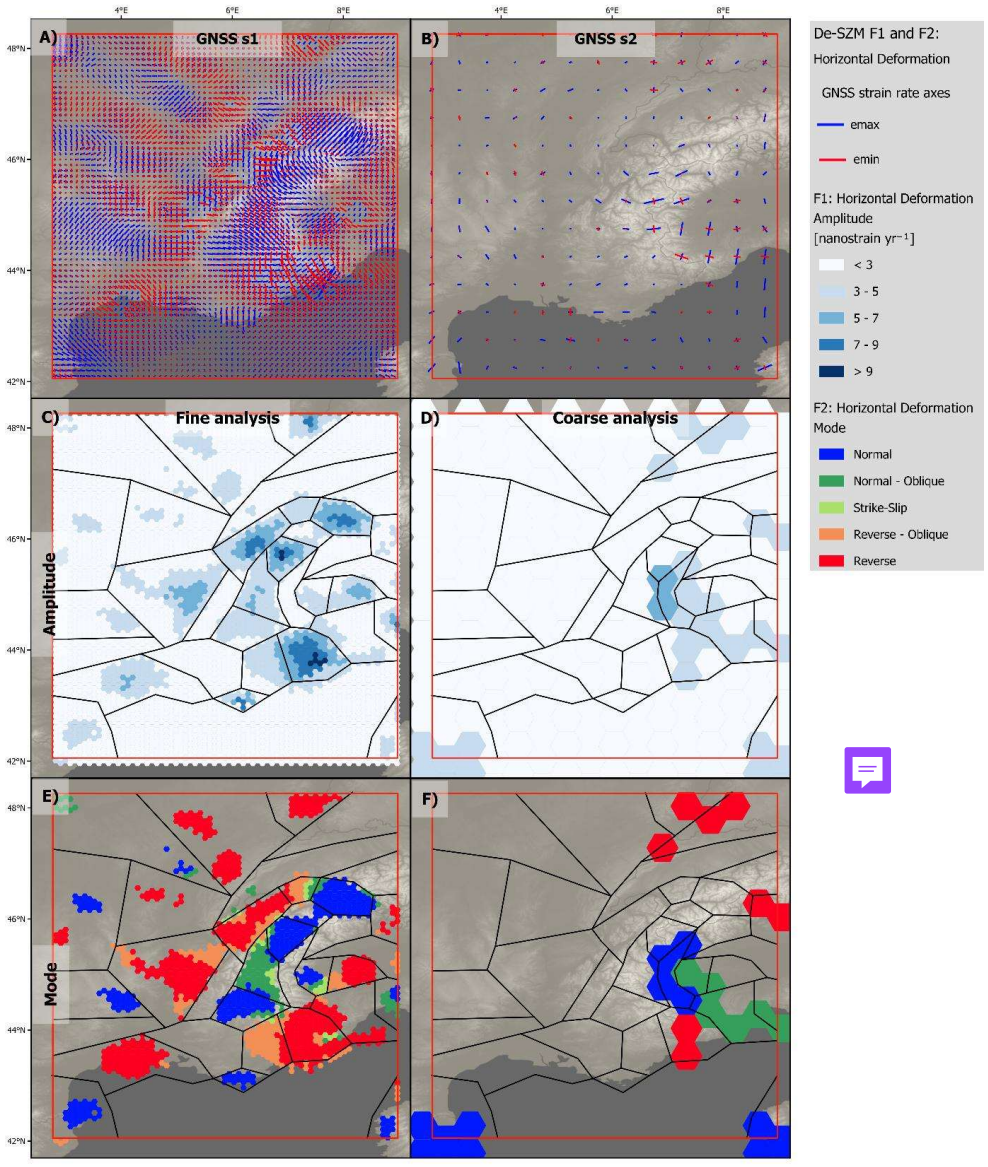

Figure 8: Geodetic data used to characterize F1 (horizontal deformation amplitude) and F2 (horizontal deformation mode) of the deformation-based SZM. A), B) Maximum and minimum strain axes from the GNSS strain solutions 1 and 2, respectively (GNSS s1: Piña-Valdés et al., 2022, GNSS s2: Lantmäteriet, 2023). C), D) Horizontal deformation amplitude for both respective GNSS solutions, for cells of the fine and coarse grid, respectively; E), F) Horizontal deformation mode for both respective GNSS solutions, for cells of the fine and coarse grid, respectively. C) to F) are superposed with the resulting zone limits of the De-SZM.

F3: Vertical displacement

The datasets used to quantitatively characterize this feature are geodetic displacement rates from GNSS solutions (GNSS v1: Piña-Valdés et al., 2022, GNSS v2: Sternai et al., 2019) (Fig. 9a, 9b). Both GNSS solutions consistently identify uplift along the internal part of the Alps (up to 2.5 mm yr^{-1}) and subsidence in the peripheral basins (up to

https://doi.org/10.5194/egusphere-2026-623
Preprint. Discussion started: 5 March 2026

295 2 mm yr^{-1}), yet differing in the width of the affected uplifting area. We map the sparse point data in the coarse grid cells by attributing the mean value of velocities comprised within each cell (Fig. 9d, 9e).

To strengthen the characterization of vertical displacement we examine an InSAR uplift-rate solution (Mathey et al., 2022; Fig. 9c, 9f) from a qualitative perspective. Although InSAR advantages and limitations differ from those of GNSS, this solution overall confirms the observed patterns obtained with GNSS.

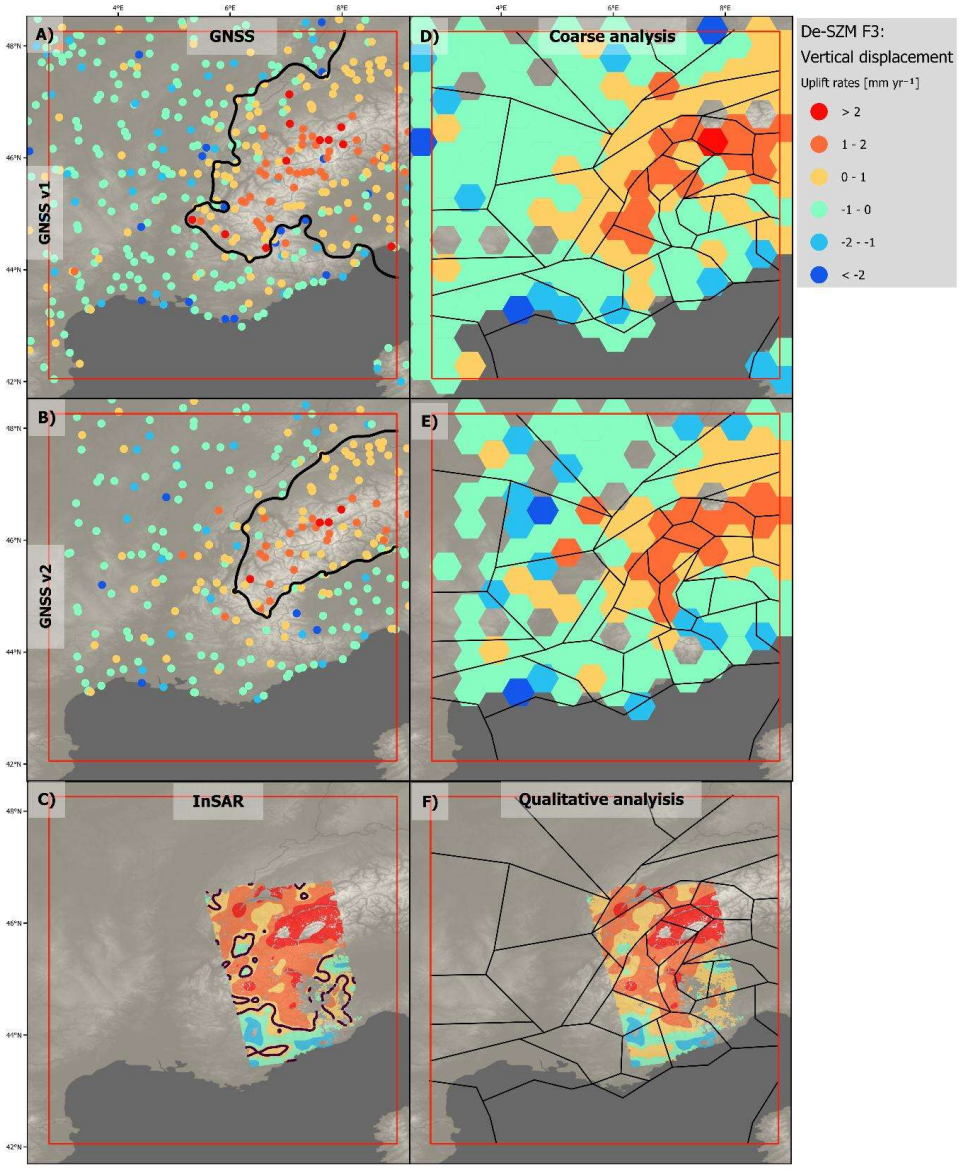

300

Figure 9: Geodetic data used to characterize F3 (vertical displacement) of the deformation-based SZM. A), B) Uplift rates for the GNSS stations included in the GNSS velocity solution 1 (GNSS v1: Piña-Valdès et al., 2022, reference frame ITRF2014) and GNSS velocity solution 2 (GNSS v2: Sternai et al., 2019, reference frame ITRF2008), respectively; C) InSAR uplift rate solution (Mathey et al., 2022, reference frame IGS14). A black line illustrates the interpolated 305 **subsidence – uplift limit for A), B) and C); D), E) Mean GNSS uplift rates for both respective GNSS solutions for cells of the coarse grid; F) InSAR uplift rate solution; D), E), F) are superposed with the resulting zone limits of the De-SZM.**

https://doi.org/10.5194/egusphere-2026-623
Preprint. Discussion started: 5 March 2026

4. Zone delineation and zone limit confidence levels

4.1 Structural-based Seismotectonic Zonation Model

From a practical sequential viewpoint, we delineate zones after the surface and in-depth geology (F1). As a second step we overlap the resulting zones with the SEFPAF fault catalog (F2) and remap the zones in order to coherently respect structural differences. Afterwards, we check that each fault from the fault-based source model for SHA (Mowbray et al., 2025) is preserved entirely within a zone and that its prolongation in depth is considered. At last, we modify the zones to consistently integrate the geometry of the crust given by the Moho depth (F3). The final zonation is then revisited by each of the features in order to remain consistent, conserving data homogeneity within the zones.

We characterize zones after the most representative values for each observable (Fig. 10, Table B1); for geology (F1) we identify the main geological Era corresponding to the units observed on surface, and the thickness of the Mesozoic - Cenozoic basin cover; for faults (F2), we note the most illustrative azimuth, the quantity of fracture - low, mean, high -, the maximum seismogenic potential index given by SEFPAF, and the presence of a major structure according to the fault source model derived from SEFPAF; for crustal thickness (F3), we note the most representative crustal thickness range. Subsequently we compute the normalized sum of differences of the three key features ($\sum\Delta F_i$, see *Code and data availability*) among neighboring zones in order to attribute confidence levels to zone limits. With the intention of obtaining an equitable distribution of the three levels of confidence we establish, for this model, low confidence levels when $\sum\Delta F_i < 0.15$, intermediate confidence levels when $0.15 < \sum\Delta F_i < 0.4$, and high confidence levels when $0.4 < \sum\Delta F_i < 1$.

We obtain 44 zones for this model with 13 zone limits with associated high confidence level, 45 limits associated with intermediate confidence level and 25 limits with low confidence level (Fig. 10). The data and feature values per zone are captured in the database of the Structure-based SZM (Table B1).

https://doi.org/10.5194/egusphere-2026-623
Preprint. Discussion started: 5 March 2026

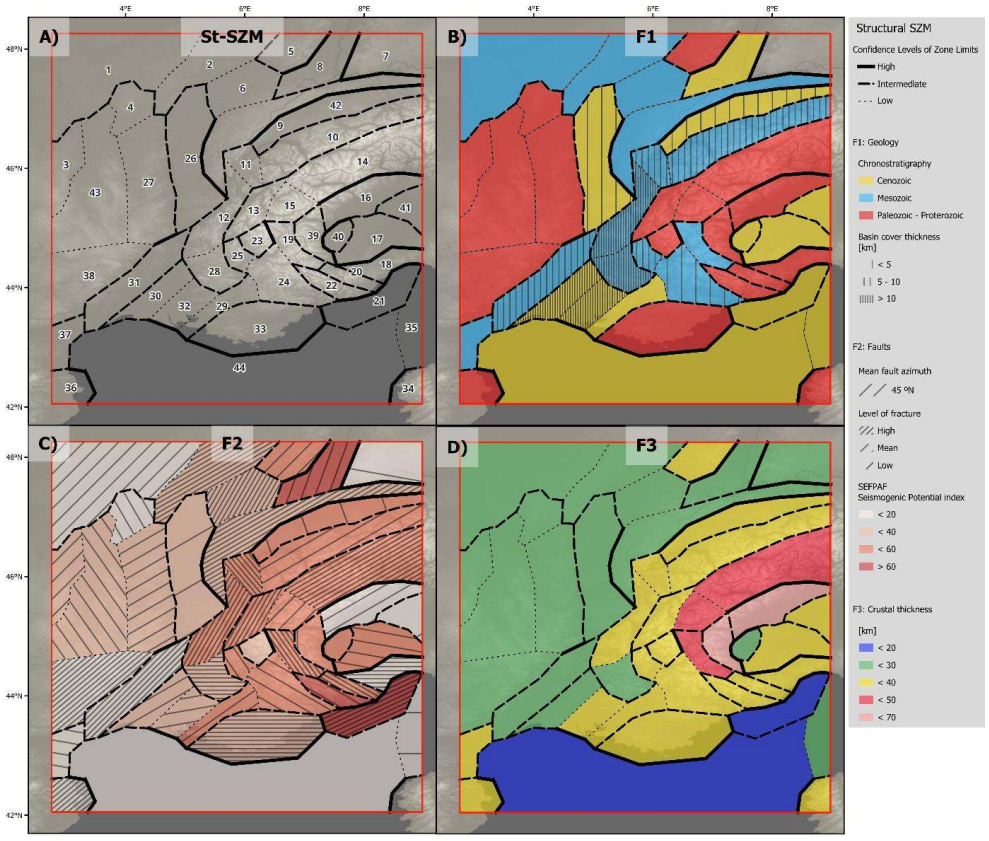

Figure 10: A) Structure-based seismotectonic zonation model with zone id values and with 3 different levels of zone limit confidence; B), C) and D) Values for F1, F2, and F3 per zone of the structural-based seismotectonic zonation model, respectively.

4.2 Seismicity-based Seismotectonic Zonation Model

Following the approach described for the structure-based SZM, we delineate zones for the seismicity-based model after the distribution of feature categories in the following order of observation: seismic flux (F1), rupture mechanism (F2) and seismogenic depth (F3). At the end of the process, we revisit all the features with their respective datasets to verify zone consistency.

Next, we assign the CLZL by quantifying the feature heterogeneity among neighboring zones. Firstly, we compute the feature values (F1, F2, F3; Fig. 11; Table B2) from each dataset within each zone, as computed previously for the grid cells. We then calculate the weighted average feature value per zone, by applying the dataset contribution weights expressed in Table 1. Last, we assess the confidence level of zone limits by normalizing the sum of differences of the three key features ($\sum\Delta F_i$) among zones sharing a boundary. For this model we establish low confidence levels when $\sum\Delta F_i < 0.3$, intermediate confidence levels when $0.3 < \sum\Delta F_i < 0.6$, and high confidence levels when $0.6 < \sum\Delta F_i < 1$.

We delineate 37 zones for this model obtaining 13 limits of high confidence, 46 limits of intermediate confidence and 26 limits of low confidence (Fig. 11). The data and feature values per zone are captured in the database of the Seismicity-based SZM (Table B2).

https://doi.org/10.5194/egusphere-2026-623
Preprint. Discussion started: 5 March 2026

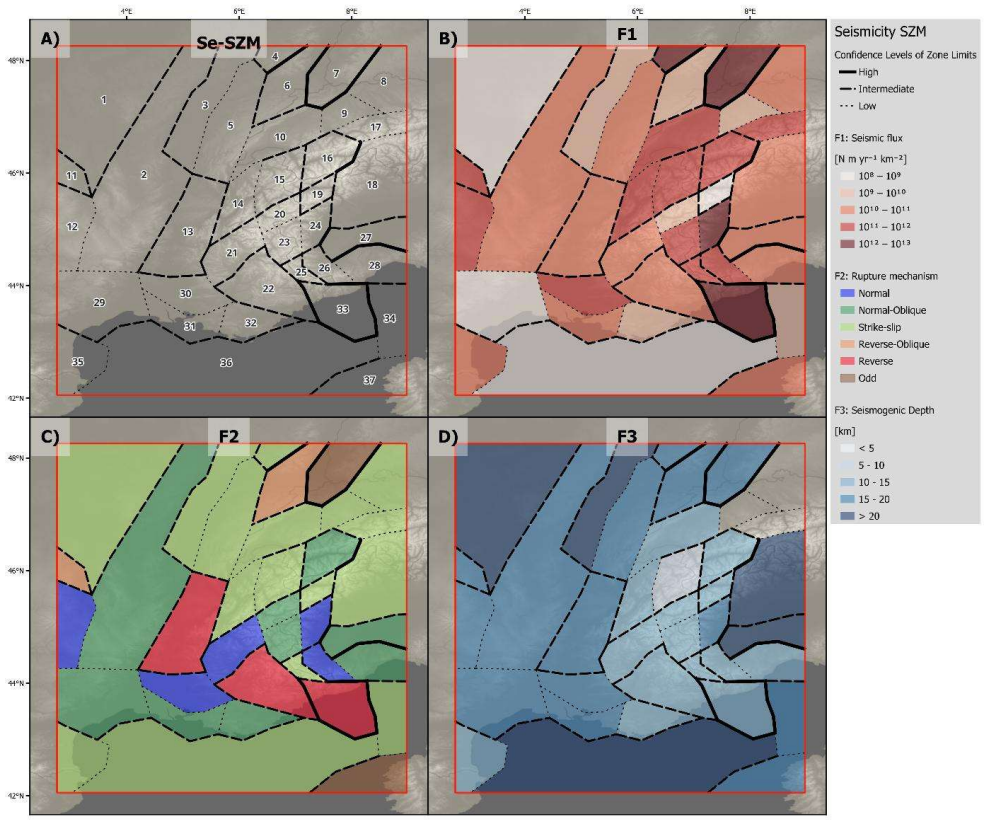

Figure 11: A) Seismicity-based seismotectonic zonation model with zone id values and with 3 different levels of zone limit confidence; B), C) and D) Mean weighted values for F1, F2, and F3 per zone of the seismicity-based seismotectonic zonation model, respectively.

4.3 Deformation-based Seismotectonic Zonation Model

We follow the same procedure as described in 4.1 and 4.2 and delineate zones for the deformation-based model after the spatial distribution of each considered feature, starting with the horizontal deformation amplitude (F1), followed by the horizontal deformation mode (F2), and concluding with the vertical displacement (F3). We characterize zones with similar feature values after repeatedly examining each dataset from each feature.

With the purpose of assigning CLZLs we compute the values for each dataset per zone, and proceed by calculating a weighted average per feature (Table B3) using the contribution weights expressed in Table 1. At last, we obtain a confidence level for each zone limit by normalizing the sum of differences of the three key features ($\sum\Delta F_i$) among the zones on each side of a boundary. For this model we establish low confidence levels when $\sum\Delta F_i < 0.15$, intermediate confidence levels when $0.15 < \sum\Delta F_i < 0.35$, and high confidence levels when $0.35 < \sum\Delta F_i < 1$.

This model presents 35 zones with 18 limits of high confidence, 41 limits of intermediate confidence and 17 limits of low confidence (Fig. 12). The data and feature values per zone are captured in the database of the Deformation-based SZM (Table B3).

https://doi.org/10.5194/egusphere-2026-623
Preprint. Discussion started: 5 March 2026

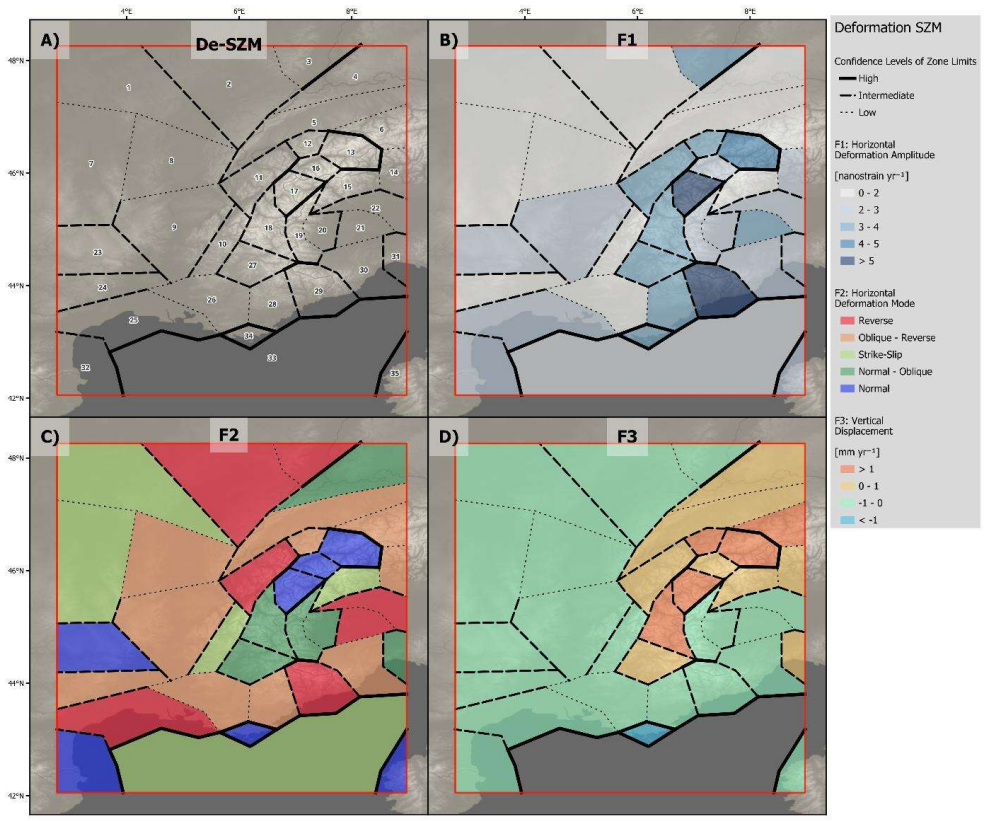

Figure 12: A) Deformation-based seismotectonic zonation model with zone id values and 3 different levels of zone limit confidence; B), C) and D) Mean weighted values for F1, F2, and F3 per zone of the deformation-based seismotectonic zonation model, respectively.

4.4 Unified Seismotectonic Zonation Model

With the aim of building a single model which integrates all three seismotectonic aspects (crustal structure, observed seismicity, geodetic deformation) and thus includes all the features listed in this work, we produce a model named "Unified Seismotectonic Zonation Model" which integrates the zone limits of the previous three.

To do this, we superpose the three SZMs (structure, seismicity and deformation-based models) and examine zone limits of significant confidence level and limits that appear consistent across multiple models (Fig. 13). We proceed by delineating zones for the unified SZM representative of zone limit recurrency and of limits presenting intermediate to high confidence levels. This strategy avoids producing one model from the processing of a large variety of data at once, instead, it relies on spatial limits already determined and on their uncertainty. Figures 13b, 13c and 13d illustrate the visual choices of zone delineation for the Unified SZM from the former SZM zone limits.

Following this confidence-based zone limit merge we improve efficiency and ensure the reflection of the strongest signals from the 3 seismotectonic feature classes: crustal structure, observed seismicity and surface deformation. The unified model is a robust SZM, especially where relevant signals are available. However, where geophysical data acquisition is sparse and seismicity and deformation rates are low, the zone delineation remains questionable. Nevertheless, it is important to note that the procedures applied to derive CLZL differ for each model, making their direct horizontal merging debatable. This implies a preferential weight towards models presenting a larger amount of intermediate and high CLZL.

https://doi.org/10.5194/egusphere-2026-623
Preprint. Discussion started: 5 March 2026

In order to compute CLZL for the Unified model we assess the difference of the nine features considered in this study (F1, F2, F3 from the St-SZM, Se-SZM and De-SZM) among zones sharing a boundary. For this purpose, we determine the observable values of the Structural-based SZM features – surface geology, basin cover thickness, mean fault azimuth, level of fracture, fault seismogenic potential index, presence of a modeled fault as a composite seismogenic source, crustal thickness – for each zone by visual expertise (Fig. B1). Subsequently we compute the Seismicity-based and Deformation-based features – seismic flux, rupture mechanism, seismogenic depth, horizontal deformation amplitude, horizontal deformation mode, vertical displacement - per zone (Fig. B1). At last, we normalize the summed difference of all nine features ($\sum\Delta F_i$) and attribute a low confidence level to $\sum\Delta F_i < 0.15$; intermediate confidence level to $0.15 < \sum\Delta F_i < 0.3$; high confidence level to $0.3 < \sum\Delta F_i < 1$.

This model presents 42 zones with 37 limits of high confidence, 52 limits of intermediate confidence and 7 limits of low confidence (Fig. 13a).

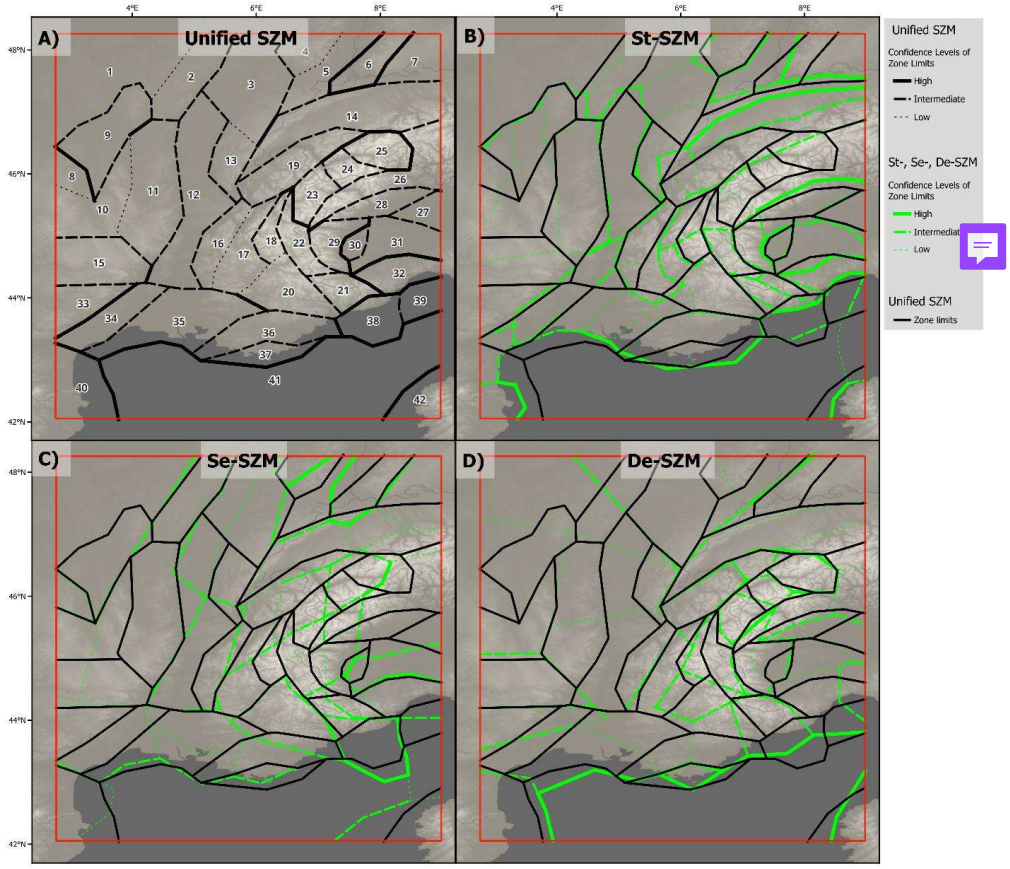

Figure 13: A) Unified seismotectonic zonation model with zone id values and 3 different levels of zone limit confidence; B), C) and D) Structure, Seismicity and Deformation-based seismotectonic zonation models, respectively showing zone limits in green with CLZL hierarchization, all three superposed with the Unified seismotectonic zonation model limits in solid black.

5 Discussion

5.1 Coherencies and discrepancies among SZM

https://doi.org/10.5194/egusphere-2026-623
Preprint. Discussion started: 5 March 2026

A comparative analysis reveals significant consistencies among the three independent seismotectonic zonation models (SZM, Fig. C1) presented in this work: structural-based, seismicity-based and deformation-based seismotectonic zonation model (St-SZM, Se-SZM, De-SZM).

In the northern-east part of the study area, elongated NE-SW oriented zones are consistently identified in both St-SZM and Se-SZM, capturing the Rhine graben structure, while geodetical constrains illustrate only the eastern edge of this structure. The western sector shows moderate size zones across all models, with comparable zone boundaries among the St-SZM and De-SZM. Robust feature differences appear along the margin of the Eastern Pyrenees allowing for a similar and confident zone delineation for the three models.

For the southern section, the Mediterranean Sea exhibits distinct zone delineation across the three SZM, mostly reflecting limited geophysical and geological data coverage. Low-confidence zone limits along the meridian 8º are identified in both Se-SZM and St-SZM, representing coherent yet small seismotectonic behavioral change across both models. All three SZM consistently identify independent seismotectonic zones for Corsica and the Var region, although zone geometries differ. The Ligurian fault zone is illustrated by high confidence limits in both St-SZM and Se-SZM, however, not reflected by geodetic signals. In contrast, the area between eastern Cevennes and Var region displays a clear structural framework dominated by major fault systems (Cevennes, Nimes, Salon-Cavaillon, Middle Durance), yet not reflected by seismic nor geodetic features.

In the eastern part of the study area, the Po plain is subdivided into multiple zones and consistently separated from the Maritime Alps across all SZM, at slightly differing latitudes. An E-W central subdivision of the Po plain, occasionally arch-shaped following the Po fault geometry, is common to all models. Zones representative of the Ivrea mantle body are consistent across the St-SZM and the De-SZM, while the Briançonnais seismic arc is illustrated across all three SZM with varying zone geometries. More broadly, the Alpine arc, Jura Mountain range and Swiss Molasse basin, are well captured in all models, with differing levels of internal subdivision.

Larger discrepancies among models occur in the central area of the study zone, where dense and variably oriented zone boundaries reflect complex structural patterns and poorly correlated geodetic and seismic signals. We conclude that structural, seismic and geodetic signals are most coherent along the Eastern Pyrenees, Var region, Corsica, Po plain, Alpine arc, Swiss Molasse basin, Jura Mountain range and the Rhine graben. These multifeatured signals may be linked to specific faulting or deformation mechanisms which lie beyond the scope of this study.

5.2 Comparison with previous zoning schemes for France

The first seismogenic source model (SSM) published for metropolitan France is a seismotectonic zonation model (EPAS model – Autran et al., 1998), presenting already different levels of consolidation for zone limits. This model has been used in numerous PSHA studies (Martin et al., 2002; Beauval and Scotti, 2004; Clément et al., 2004; Beauval et al., 2006; Secanell et al., 2008; Woessner et al., 2015). An important update of this model was published in 2013 (Baize et al., 2013), introducing the classification of data into dynamic (seismicity and deformation) and static (structural) observations. The Baize et al. (2013) model has been used in many subsequent PSHA studies (Chartier et al., 2017; Martin et al., 2018; Drouet et al., 2020; Beauval et al., 2020; Danciu et al., 2024). Since then, several propositions to update this zoning have been done, especially from the industrial sector (e.g., Martin et al., 2018; Le Dortz et al., 2019), each of them acknowledging the need for updating SZMs given the fast increase of available seismotectonic and geophysical data.

In the following we discuss and illustrate the differences among three previously compiled seismotectonic zonation models (Autran et al., 1998; Baize et al., 2013; Le Dortz et al., 2019) and the unified SZM proposed in this study (Fig. 14). The objective is to highlight the new contributions arising from the sequential methodology and the updated dataset implemented in the present work. We recognize main structural elements along most of the models (e. g. Eastern Cevennes, Rhone valley, Western Alpine front, Rhine graben, Jura Mountain range, Swiss Molasse basin, Po plain, Ligurian fault zone, Digne arc, Var region, Gulf of Lyon; Fig. 14), yet many of the boundaries differ where the geological structure is less clear and where seismicity and deformation rates are low.

The EPAS model (Autran et al., 1998) incorporates stress, deformation, and seismic distribution, as well as structural components. However, this model underlines the influence of tectonic domains, reflecting major faults as zone boundaries. It also proceeds by building sequenced SZM which are at last complemented to form one only

https://doi.org/10.5194/egusphere-2026-623
Preprint. Discussion started: 5 March 2026

model, each giving place to a hierarchy of zone boundaries. The 1st model is built on major crust structure and geodynamics, the 2nd model is based after deformation data – stress field and neotectonic evidences - and, the 3rd model follows the seismicity distribution.

We identify similarities among the ESHM13 model (Woessner et al., 2015, modified from Autran et al., 1998 for the French territory; Fig. 14a) and the structural and deformation feature patterns presented in this study. In both models the Rhine graben region presents multiple zones oriented SSW – NNE; the Alpine arc presents smaller zones that follow the arcuate shape of the chain; the Cevennes region and Rhone valley present comparable zone delineations. However, the northwestern part of the study area presents larger zones - reflecting the diffuse nature of seismicity and deformation and the difficulty to distinguish reliable seismotectonic features here.

The Baize et al. (2013) model (Fig. 14b) integrates with detail structural and geological surface features, with zone boundaries also following major known faults. This study dissociates seismotectonic features into static (geology) and dynamic (seismotectonics, neotectonics) data. It integrates the distribution of instrumental and historical seismic events (Mw > 5.5) from Sisfrance, Rénass and CEA/LDG, a stress regime from focal mechanisms (Heidbach et al., 2010), neotectonic evidences (0 – 10 Ma; Baize et al., 2002; Bertrand et al., 2007) and, the Miocene – Pliocene deformation pattern and distribution. Yet, we identify the structural geology as the most impacting feature for this model and observe major resemblances with the structure-based SZM presented in this study, without many similarities with the seismicity or deformation-based SZM. Baize et al. (2013) also developed a hierarchical classification of zone boundaries in 4 orders: the 1st order reflects zonation based on geodynamic history, significant structures and seismic density; the 2nd order builds zones where several dynamic criteria converge; the 3rd and the 4th order are based on discrete criteria.

The third model (Le Dortz et al., 2019; Fig. 14c) is an update of the EPAS model developed during the last two decades by GEOTER. It delineates zone boundaries after crustal transition zones from tomographic and gravimetric data, surface geology, the BDFA fault catalog (Jomard et al., 2017) and, the World Stress map (Heidbach et al., 2016). They classify data into static and dynamic parameters as done in Baize et al. (2013). This work classifies zone boundaries into three levels, each after specific observations: the major boundaries correspond to the Moho discontinuities; the secondary boundaries to secondary crustal transition zones and the limit between continental and crustal crust; the third-level boundaries are defined after stress regime and faults. This model contrastively presents little zone limit resemblance with any of the 4 SZM presented in this study. Yet, major tectonic domains can be distinguished.

The comparison of the Unified SZM with previous seismotectonic zonation models strongly illustrates the impact of integrating active deformation and seismic observations from newly available geophysical data. The zoning approach presented here indeed integrates structural, seismic and geodetic features, while previous models primarily capture structural and crustal stress parameters, and are thus less influenced by seismic and deformation observations.

https://doi.org/10.5194/egusphere-2026-623
Preprint. Discussion started: 5 March 2026

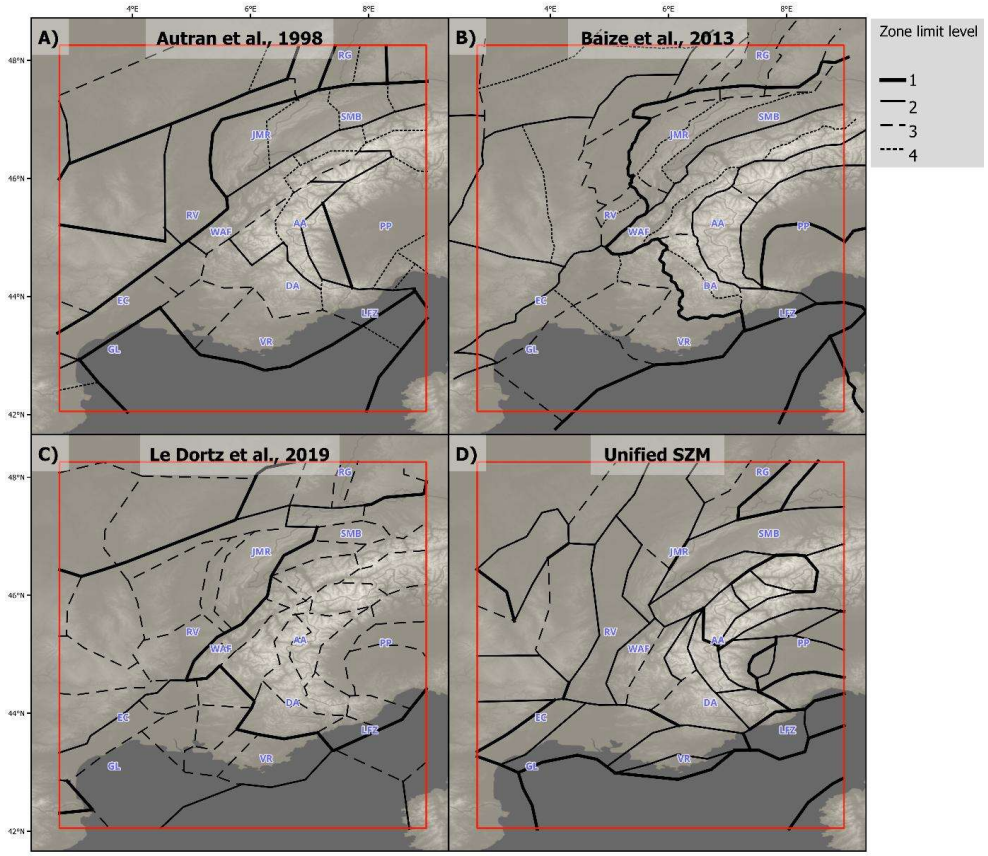

Figure 14: A), B) and C) Previous seismotectonic zonation models (Autran et al., 1998; Baize et al., 2013; Le Dortz et al., 2019, respectively) presenting three to four different levels of zone limits.; D) The Unified seismotectonic zonation model from this study presenting the 3 levels of zone limit confidence. Geographic regions are labeled for reference: RG: Rhine graben, SMB: Swiss Molasse basin, JMR: Jura Mountain range, WAF: Western Alpine front, RV: Rhone valley, EC: Eastern Cevennes, GL: Gulf of Lyon, VR: Var region, DA: Digne arc, LFZ: Ligurian fault zone, AA: Alpine arc, PP: Po plain.

5.3 Handling seismic source characterization uncertainties

There are inherent uncertainties in the definition of source zone models for seismic hazard assessment. In the case of South-East France, our current seismotectonic knowledge is limited due to low-moderate seismicity levels, slow deformation rates, limited time periods of geophysical recordings to confidently characterize seismic patterns and surface deformation, alongside limited active fault knowledge. Building seismic source models (SSM) using up-to-date geophysical and geological data, along with a deep understanding of the regional seismotectonics and of the considered data partly allows to mitigate uncertainties. Furthermore, combining in a logic-tree multiple SSM, preferentially developed at regional/local scale, allows to explore and reduce some of the uncertainties (Hashemi et al., 2023, 2024).

In this work we present four sequenced SZM for the region of South-East France which reflect the current state of knowledge on seismic source characterization. Uncertainties related to zone delineation are reduced by grouping seismotectonic parameters into categorical groups, thus diminishing complexity of zone mapping and ensuring data signals are adequately expressed in the final model. Zone boundaries are subsequently evaluated by quantifying the feature contrasts across each zone limit. Nevertheless, residual expert-opinion related uncertainties

https://doi.org/10.5194/egusphere-2026-623
Preprint. Discussion started: 5 March 2026

arise from methodological choices, such as the selection of datasets for feature characterization, weighting schemes used to derive feature averages, the sequencing of feature and dataset analysis during zone delineation, and the definition of cumulative feature-difference ($\sum\Delta F_i$) levels used to attribute CLZL.

Moreover, underlaying data-intrinsic uncertainties, such as heterogeneous data density, uncertainties linked to data acquisition or linked to physical assumptions, influence the resulting zone mapping, the CLZL values and, consequently the contribution of each SZM to the final unified model. More explicitly, data-related uncertainties affect several key datasets. Structural data are subject to uncertainties regarding the current state of knowledge on faults and their potential seismic activity. Seismic records are affected by uncertainties in macroseismic magnitude and location estimates, limited periods of catalog completeness, inconsistencies of magnitude estimate among different seismic catalogs, uncertainties in hypocentral depth and, biases introduced by event density which influence the estimation of seismogenic depth and rupture mechanism – related to the time and space heterogeneity of instrumental coverage. Geodetic solutions are also impacted by uncertainties arising from methodological assumptions in velocity and strain estimation, as well as from the relatively short duration of available observational time series, while they may also capture aseismic deformation.

The impact of the features and datasets used to develop a SZM is dependent on the availability, reliability, density and continuity of the data. Therefore, where one dataset presents little representation, the remaining datasets will take on a higher role for zone delineation. On the contrary, where observations are redundant, SZM models appear more robust.

Including the three independent SZM as alternative models populating a logic tree in a seismic hazard study allows for a more comprehensive evaluation of epistemic uncertainties. In previous SHA studies the integration of alternative models produced by different authors compensates the diverse uncertainties linked to expert opinion choices; here, we suggest to examine uncertainties by quantitatively evaluating zone delineation choices. This approach explicitly acknowledges that no single model can reliably forecast future earthquakes on its own.

Moreover, we aim for the reproducibility of the sequenced seismotectonic zonation method presented in this work by evoking transparently the methodology and making accessible the code and data used to obtain the four SZM (10.5281/zenodo.18391170, Mowbray et al., 2026, see *Code and data availability*). In this line, future updates can easily be applied in the case of new geophysical acquisitions or reconsideration of ponderation weights or feature prioritization. A long-term objective is to integrate the depth component of the considered data (e.g. focal mechanisms, geology, seismogenic depth) in order to build a 3D seismotectonic zonation model which considers in depth seismotectonic variations.

With the objective of building seismogenic source models for PSHA from the SZM, magnitude-frequency distributions will need to be derived for the zones of each model. Depending on the catalog used, some of the zones may comprise too few events to reliably establish this distribution. In this case, the confidence levels associated to the zone limits may be used to take decisions on the merging of zones and the creation of larger source zones. Large zones may compensate the short observation windows of seismic records, assigning plausible recurrence rates to zones for which no events have been observed in the past.

6 Conclusions

Characterizing seismic sources in low to moderate seismic regions, such as South-East France, is a scientific challenge which demands a multidisciplinary analysis of local seismotectonics. We develop three alternative and independent seismotectonic zone models (SZM) which robustly rely on distinct seismotectonic features, grouped into three themes, each offering a different insight to seismic hazard; geology and crustal structure, observed seismicity and geodetically observed surface deformation. Additionally, we introduce a fourth model, the unified seismotectonic zonation model, which encompasses all the observations considered within the three thematic models.

The seismotectonic zonation models presented here differ from previous zonation efforts for the region through multiple aspects: the disaggregation of seismotectonic features into thematic groups, the expanded spatial and temporal coverage of geophysical records, the integration of seismic data from cross-border countries, the increased consideration of geodetically constrained surface deformation and, the quantitative evaluation of zone delineation based on feature heterogeneity. The limitations of this work are principally linked to data-related

https://doi.org/10.5194/egusphere-2026-623
Preprint. Discussion started: 5 March 2026

uncertainties, the temporal and methodological heterogeneity of datasets to characterize one same feature (e.g. different seismic catalogs, different geodetic solutions), the limited temporal observation windows of geophysical data and, expert-opinion methodological choices (e.g. ponderation weights for datasets).

Moreover, we introduce a novel methodology for zone boundary hierarchization, which assesses quantitatively the variability of each feature within a model and avoids boundary level attribution to one specific observation. Our strategy apports objectivity and allows for a maximum use of seismotectonic data. The resulting models can be used in a source model logic tree, thus, the uncertainty on which model is most accurate for forecasting future earthquakes is propagated up to hazard estimates. Our approach is reproducible and enables the updating of seismotectonic zonation models as new geophysical data become available. However, variability related to the author's expert choices will inevitably persist.

Advances in the geophysical framework alongside the temporal extension of geophysical records, allow for a more comprehensive description of the current crustal deformation and its incorporation into seismic source models for SHA. Nevertheless, seismic source characterization remains limited in regions with sparse geophysical instrumentation and weak seismic or geodetic signals. Therefore, seismic source characterization will continue to improve with geophysical instrumentation deployments and the accumulation of long-term measurements.

https://doi.org/10.5194/egusphere-2026-623
Preprint. Discussion started: 5 March 2026

Appendices

Appendix A: Seismic catalog completeness period estimations

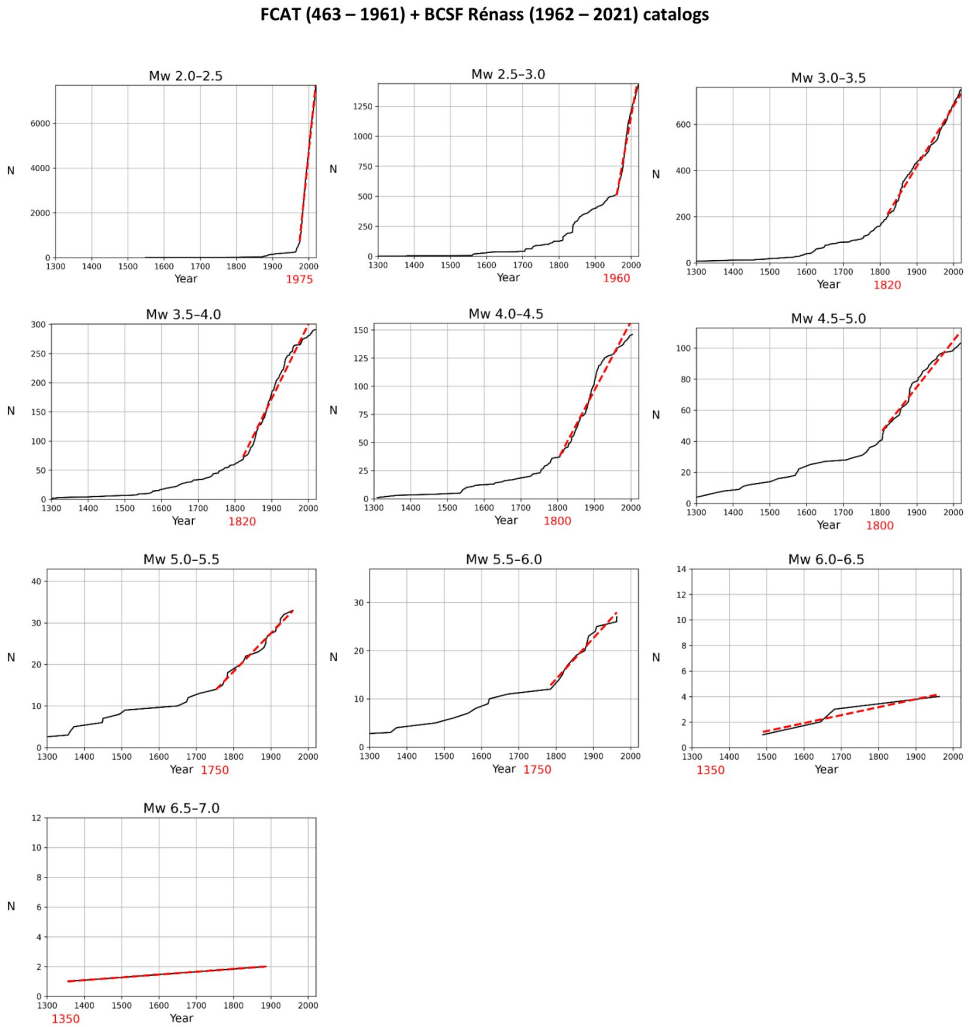

Figure A1: Assessment of completeness periods for magnitude bins of Mw 0.5 for the FCAT (463 – 1961; Manchuel et al., 2018) + BCSF Rénass (1962 – 2021; BCSF Rénass, 2022) catalogs, by finding the inflection point of constant cumulative number of events (N) in time. Considering events falling within the area of interest (solid red rectangle in Figure 1).

https://doi.org/10.5194/egusphere-2026-623
Preprint. Discussion started: 5 March 2026

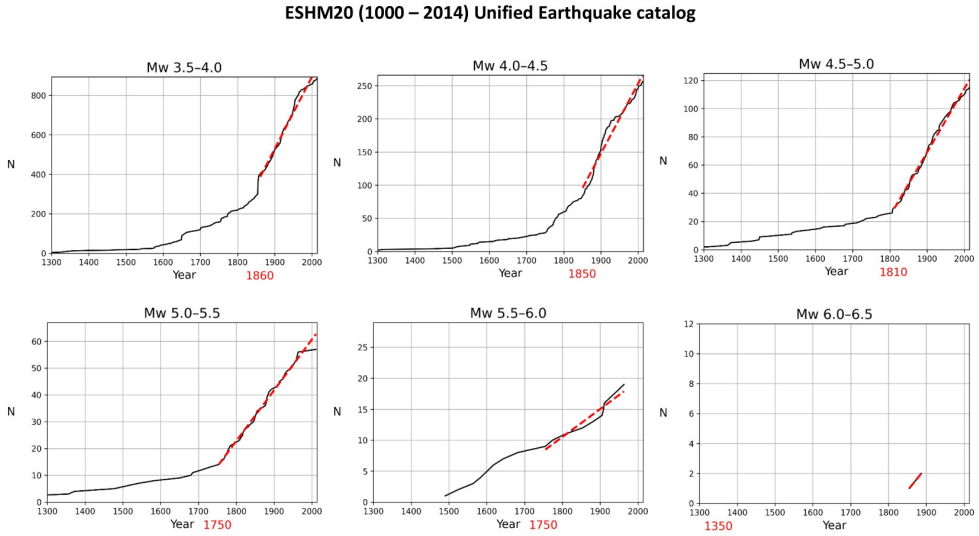

595 **Figure A2: Assessment of completeness periods for magnitude bins of Mw 0.5 for the ESHM20 Unified Earthquake catalog (1000 – 2014, Danciu et al., 2024), by finding the inflection point of constant cumulative number of events (N) in time. Considering events falling within the area of interest (solid red rectangle in Figure 1).**

Appendix B: Seismotectonic features for zones of each SMZ

id	F1: Geology		F2: Faults				F3: Crustal Thickness
	Surface	Cover thickness (km)	Mean azimuth (ºN)	Level of fracture	SP index	Model fault	Crustal thickness (km)
1	Meso		45	Mean	< 20		20 – 30
2	Meso		60	High	< 40		20 – 30
3	Paleo	0	45	Mean	< 40		20 – 30
4	Paleo	0	150	Mean	< 20		20 – 30
5	Paleo	0	45	Mean	< 60		30 – 40
6	Meso		30	High	< 40		20 – 30
7			100	Low	< 20		20 – 30
8	Ceno		20	Mean	> 60	Jura Front	20 – 30
9	Meso		60	High	< 40	Jura Front	20 – 30
10	Meso-Ceno	7	60	Mean	< 60	Alpine Front N	30 – 40
11	Meso-Ceno	6	140	High	< 60	Vuache	30 – 40
12	Meso	10	30	High	< 60	Alpine Front S	30 – 40
13	Paleo	0	30	High	< 60	Belledonne	30 – 40
14	Paleo	0	60	High	< 60	Rhone + Aosta	40 – 50
15	Paleo	0	45	Mean	< 60	Valloire	40 – 50
16	Paleo-Ceno		60	Mean	< 20		50 – 60
17	Ceno		100	Mean	< 60	Po Thrust	30 – 40
18	Paleo	0	90	High	< 20		30 – 40
19	Meso	0	145	High	< 60	High Durance	40 – 50
20	Paleo-Meso		120	High	< 60		30 – 40
21	Ceno		65	High	> 60	Ligure	10 – 20
22	Paleo	0	120	Mean	> 60	Taggia	30 – 40
23	Paleo	0	50	Low	< 40		30 – 40

https://doi.org/10.5194/egusphere-2026-623
Preprint. Discussion started: 5 March 2026

24	Meso	4	120	Mean	< 60	Digne Arc + Parpaillon	30 – 40
25	Meso	8	145	Mean	< 60	Veynes	30 – 40
26	Ceno	2	60	Low	< 40		20 – 30
27	Paleo	0	60	Mean	< 40		20 – 30
28	Meso	10	90	High	< 40	Ventoux	20 – 30
29	Ceno		55	Mean	< 60	Middle Durance	30 – 40
30	Ceno	10	60	Mean	< 40	Nimes	20 – 30
31	Meso-Ceno	8	45	High	< 20	Cevennes	20 – 30
32	Ceno	12	80	Mean	< 40	Salon-Cavaillon	30 – 40
33	Paleo-Meso		90	High	< 40		30 – 40
34	Paleo		70	Low			30 – 40
35	Ceno		90	Low	< 20		10 – 40
36	Paleo-Prote		50	High	< 20		30 – 40
37	Meso-Ceno		100	Mean	< 20		30 – 40
38	Paleo-Prote		50	High	< 20		20 – 30
39	Paleo-Meso		180	Low	< 60	Po Thrust	50 – 60
40	Ceno		50	Low	< 60		20 – 30
41	Ceno		60	Low	< 20		30 – 40
42	Ceno	5	160	Low	< 60		30 – 40
43	Paleo-Prote		145	Mean	< 40		20 – 30
44	Ceno			Low	< 20		10 – 20

Table B1: Data and feature values for the structural seismotectonic zonation model within each zone: Surface geology (Chantraine et al., 2003), basin cover thickness (GeoMol Project Team, 2019; Bienveignant et al., 2024), mean fault azimuth, level of fracture, seismogenic potential (SP) index, presence of a modeled fault for SHA (Mowbray et al., 2025) and, crustal thickness (Nouibat, 2024, Hengl et al., 2022).

id	F1: Seismic Flux (N·m yr^{-1} km^{-2})			F2: Rupture mode	F3: Seismogenic Depth (km)			
	FCAT + BCSF	ESHM20	F1	Focal mechanisms F2	SISMALP	BCSF	ISIDe	F3
1	7.77e+08	4.47e+08	7.11e+08	Strike-slip	24.8	20.0		24.0
2	1.16e+10	7.04e+09	1.07e+10	Normal-Oblique	18.3	20.0		18.5
3	2.31e+09	5.59e+08	1.96e+09	Strike-slip	21.4	20.1		21.2
4	2.65e+12	2.09e+10	2.13e+12	Strike-slip		20.0		20.0
5	4.22e+10	9.41e+09	3.57e+10	Strike-slip	17.0	20.1		17.6
6	8.41e+09	3.47e+09	7.42e+09	Reverse-Oblique		20.0		20.0
7	1.61e+12	2.11e+12	1.71e+12	Odd		20.0		20.0
8		2.14e+10	2.14e+10	Strike-slip				
9		2.43e+09	2.43e+09	Strike-slip				
10	9.26e+10	1.53e+11	1.05e+11	Strike-slip	13.9	20.1		14.9
11	1.15e+12	4.44e+10	9.32e+11	Reverse-Oblique	19.5	20.1		19.6
12	1.91e+11	7.30e+10	1.68e+11	Normal	16.4	20.0		17.0
13	8.37e+10	1.14e+11	8.98e+10	Reverse	17.0	19.9		17.5
14	8.18e+11	3.75e+11	7.29e+11	Strike-slip	11.9	13.0		12.1
15	5.55e+11	4.39e+11	5.32e+11	Strike-slip	7.6	11.0		8.2
16	1.16e+11	2.34e+12	5.60e+11	Normal-Oblique	10.7	20.0	11.1	11.8
17		5.77e+11	5.77e+11	Strike-slip				
18		4.24e+10	4.24e+10	Strike-slip			35.9	35.9
19	5.86e+08	2.44e+09	9.57e+08	Strike-slip	14.2	17.7	11.1	13.3
20	8.68e+09	3.37e+09	7.62e+09	Normal-Oblique	11.4	12.0		11.5
21	6.68e+10	4.25e+09	5.43e+10	Normal	11.8	24.5		13.9
22	3.73e+10	1.03e+11	5.04e+10	Reverse	13.7	18.0		14.4
23	8.56e+11	3.56e+11	7.56e+11	Normal-Oblique	10.8	12.0		11.0
24	1.03e+12	1.09e+12	1.04e+12	Normal	15.8	17.0	16.1	16.0
25	1.38e+11	5.96e+10	1.22e+11	Strike-slip	11.1	13.0	12.4	11.8
26	1.20e+11	4.43e+11	1.85e+11	Normal	15.5	17.0	15.0	15.5
27	6.65e+09	1.37e+11	3.26e+10	Normal-Oblique			40.8	40.8
28	2.15e+08	8.04e+10	1.63e+10	Normal-Oblique			11.0	11.0
29	1.02e+09	2.91e+08	8.72e+08	Normal-Oblique		20.1		20.1

https://doi.org/10.5194/egusphere-2026-623
Preprint. Discussion started: 5 March 2026

30	2.75e+11	2.86e+11	2.77e+11	Normal	16.5	20.1		17.1
31	9.85e+09	1.13e+10	1.01e+10	Normal-Oblique		20.1		20.1
32	1.57e+09	2.37e+09	1.73e+09	Normal-Oblique	12.1	17.8		13.0
33	4.19e+12	1.40e+12	3.63e+12	Reverse	9.8	17.5	15.7	12.9
34	1.08e+08	6.36e+09	1.36e+09	Strike-slip		20.0	15.8	16.6
35	1.51e+10	1.14e+10	1.44e+10	Strike-slip		14.2		14.2
36	5.23e+08	7.76e+07	4.34e+08	Strike-slip		22.0		22.0
37	4.64e+10	2.96e+10	4.30e+10	Odd		19.3		19.3

Table B2: Data and feature values for the seismicity-based seismogenic zonation model within each zone. FCAT + BCSF: seismic flux obtained per zone from FCAT (1356 – 1961, Manchuel et al., 2018) and BCSF Rénass (1962 – 2021, BCSF-Rénass, 2022); ESHM20: seismic flux obtained per zone from the ESHM20 unified catalogue (1356 – 2014, Danciu et al., 2024); F1: weighted mean seismic flux; Focal mechanisms, F2: rupture mode obtained per zone from the moment tensor of the focal mechanisms (Mathey et al., 2021; Mazzotti et al., 2021); SISMALP, BCSF, ISIDe: D90 quantile obtained per zone using SISMALP (1987 – 2024, Langlais et al., 2024), BCSF-Rénass (1962 – 2021, BCSF-Rénass, 2022), ISIDe (1985 – 2023, ISIDe Working Group, 2007), respectively; F3: weighted mean seismogenic depth.

id	F1: Horizontal Deformation Amplitude (nanostrains yr^{-1})			F2: Horizontal Deformation Mode			F3: Vertical displacement (mm yr^{-1})		
	GNSS s1	GNSS s2	F1	GNSS s1	GNSS s2	F2	GNSS v1	GNSS v2	F3
1	1.61	1.26	1.54	0.32	-0.77	0.1	-0.4	-0.6	-0.5
2	2.02	1.76	1.97	-0.85	-0.91	-0.86	-0.3	-0.6	-0.45
3	3.25	2.85	3.17	-0.88	-0.99	-0.9	-0.5	-0.8	-0.65
4	1.47	2.53	1.68	0.73	-0.87	0.41	0.0	0.1	0.05
5	1.87	1.38	1.77	-0.06	-0.77	-0.2	0.5	0.3	0.4
6	2.07	1.0	1.86	-0.47	0.16	-0.34	1.1	1.5	1.3
7	1.96	1.0	1.77	0.03	-0.64	-0.1	-0.5	-0.9	-0.7
8	1.94	1.64	1.88	-0.46	-0.81	-0.53	-0.6	-0.6	-0.6
9	3.17	1.22	2.78	-0.57	-0.69	-0.59	-0.2	-0.3	-0.25
10	1.78	1.3	1.68	0.02	-0.77	-0.14	-0.2	-0.3	-0.25
11	4.73	1.0	3.98	-0.67	-0.37	-0.61	0.5	0.4	0.45
12	3.98	0.8	3.34	-0.26	-0.62	-0.33	1.8	0.9	1.35
13	5.45	0.9	4.54	0.88	-0.28	0.65	2.1	1.8	1.95
14	2.69	2.75	2.7	-0.43	-0.54	-0.45	1.2	0.4	0.8
15	1.88	1.6	1.82	0.05	-0.5	-0.06	0.9	0.6	0.75
16	3.14	1.4	2.79	0.8	1.0	0.84	0.1	1.6	0.85
17	5.59	3.1	5.09	0.91	1.0	0.93	1.3	1.0	1.15
18	4.03	3.5	3.92	0.37	0.81	0.46	1.2	1.2	1.2
19	2.25	3.5	2.5	0.4	1.0	0.52	-0.3	-0.4	-0.35
20	2.9	2.4	2.8	0.62	0.44	0.58	-0.3	0.2	-0.05
21	3.85	2.65	3.61	-0.86	0.04	-0.68	0.3	-0.4	-0.05
22	2.23	1.5	2.08	-0.67	-0.33	-0.6	-0.3	-0.2	-0.25
23	2.27	1.28	2.07	0.84	0.86	0.84	-0.3	-0.3	-0.3
24	1.24	0.8	1.15	-0.49	-0.13	-0.42	-0.1	-0.1	-0.1
25	2.64	1.34	2.38	-0.7	-0.79	-0.72	-0.7	-0.8	-0.75
26	1.72	2.3	1.84	-0.43	-0.52	-0.45	-0.3	-0.1	-0.2
27	3.45	1.45	3.05	0.63	-0.69	0.37	0.3	0.3	0.3
28	3.57	1.9	3.24	-0.47	-0.71	-0.52	-0.3	-0.3	-0.3
29	6.39	3.17	5.75	-0.63	-0.76	-0.66	-0.7	-0.5	-0.6
30	2.68	2.97	2.74	-0.73	0.23	-0.54	-0.1	-0.8	-0.45
31	2.72	2.7	2.72	0.22	0.37	0.25	0.3	-0.2	0.05
32	2.45	1.97	2.35	0.77	0.91	0.8	-0.1		-0.1
33	1.26	1.32	1.27	-0.02	-0.46	-0.11			
34	4.0	1.5	3.5	0.8	0.07	0.65	-1.9	-1.6	-1.75
35	2.34	3.3	2.53	0.64	0.92	0.7	-0.9		-0.9

Table B3: Data and feature values for the deformation seismotectonic zonation model within each zone. GNSS s1, v1: GNSS strain and velocity solution (Piña-Valdès et al., 2022) used to obtain F1, F2 and F3; GNSS s2: GNSS strain solution (Lantmäteriet, 2023) used to obtain F1 and F2; GNSS v2: GNSS velocity solution (Sternai et al., 2019) used to obtain F3; F1: weighted average horizontal deformation amplitude per zone, in nanostrain yr^{-1}; F2: weighted average

https://doi.org/10.5194/egusphere-2026-623
Preprint. Discussion started: 5 March 2026

horizontal deformation mode per zone, dimensionless values corresponding to M from equation 2; F3: weighted average vertical displacement rate per zone, in mm yr^{-1}.

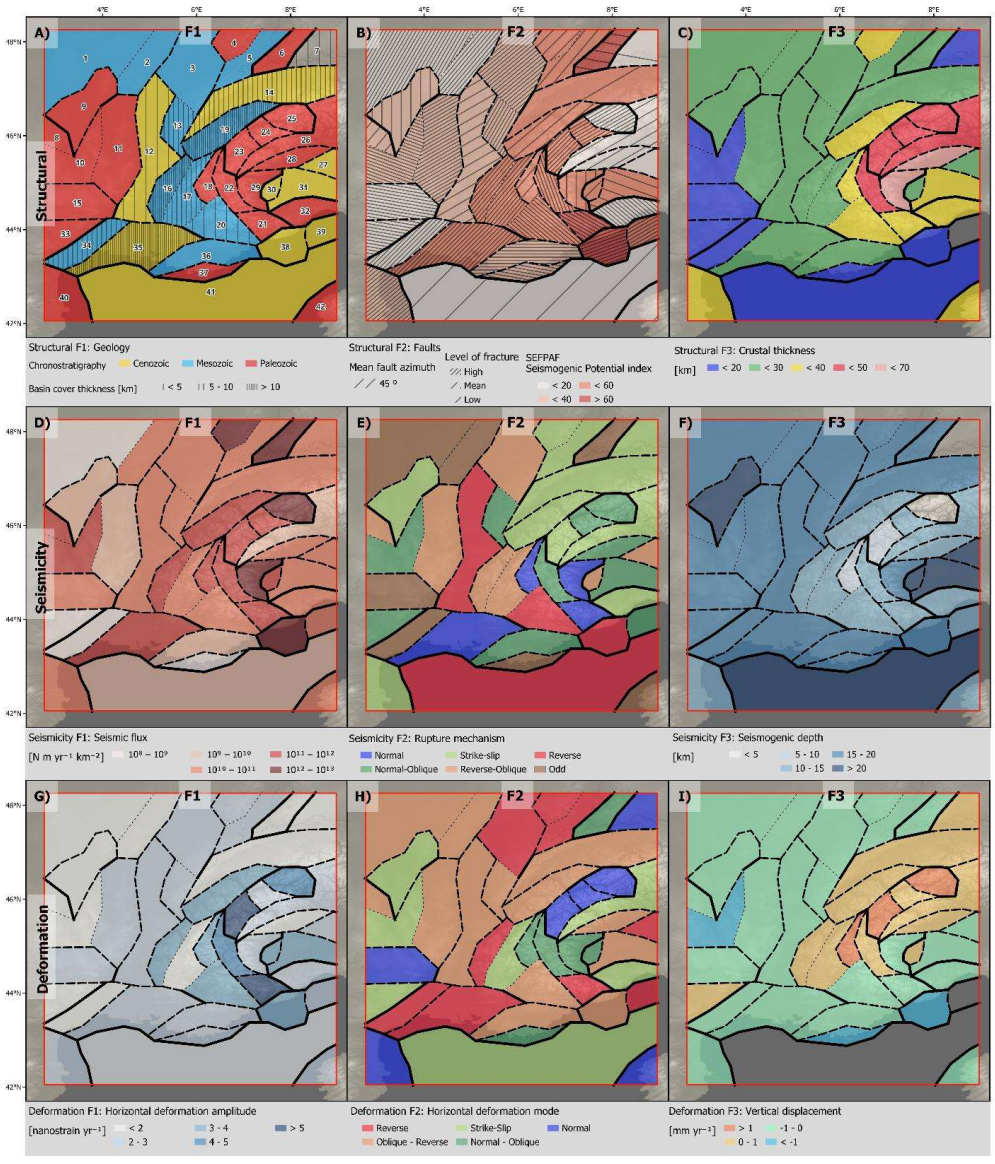

Figure B1: Unified Seismotectonic Zonation Model with CLZL per zone boundary and the characterization per zone of the 9 seismotectonic features included in this study. A) Structural feature 1 (geology) and zone id values; B) Structural feature 2 (faults); C) Structural feature 3 (crustal thickness); D) Seismicity feature 1 (seismic flux); E) Seismicity feature 2 (rupture mechanism); F) Seismicity feature 3 (seismogenic depth); G) Deformation feature 1 (horizontal deformation amplitude); H) Deformation feature 2 (horizontal deformation mode); I) Deformation feature 3 (vertical displacement).

https://doi.org/10.5194/egusphere-2026-623
Preprint. Discussion started: 5 March 2026

Appendix C: Coherencies and discrepancies among SZM

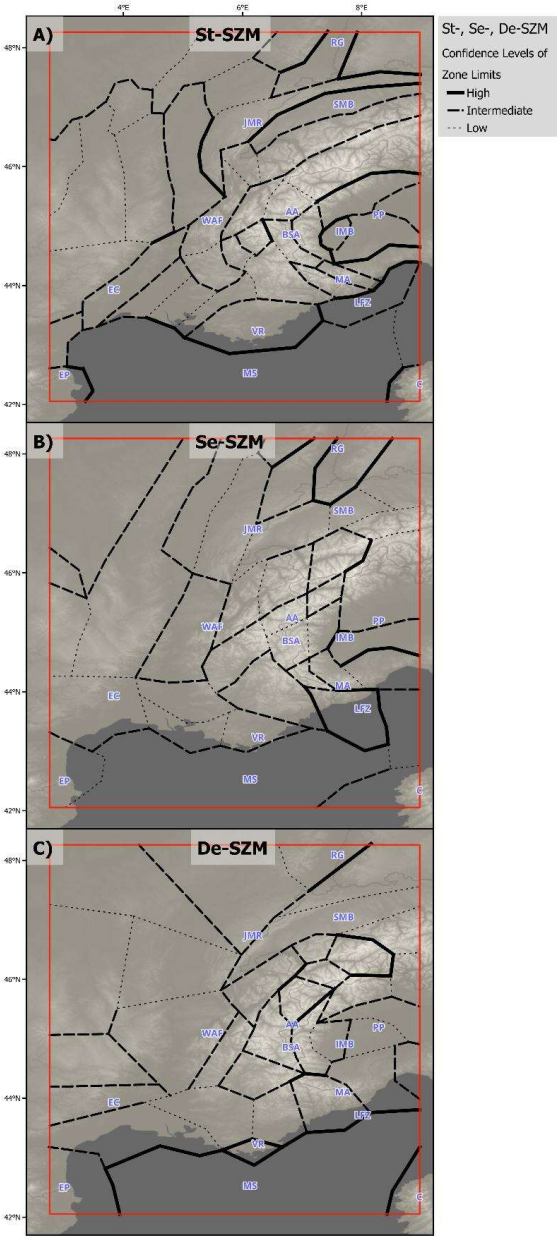

Figure C1: Spatial comparison of the three individual seismotectonic models from this study. A) B), and C) Structure, Seismicity and Deformation-based seismotectonic zonation models, respectively, showing zone limits with CLZL hierarchization. Geographic regions are labeled for reference: RG: Rhine graben, SMB: Swiss Molasse basin, JMR: Jura Mountain range, RV: Rhone valley, EC: Eastern Cevennes, EP: Eastern Pyrenees, VR: Var region, MS: Mediterranean Sea, C: Corsica, MA: Maritime Alps, LFZ: Ligurian fault zone, BSA: Briançonnais seismic arc, AA: Alpine arc, IMB: Ivrea mantle body, PP: Po plain.

https://doi.org/10.5194/egusphere-2026-623
Preprint. Discussion started: 5 March 2026

Code and data availability

The code and data used to produce the Sequenced Seismotectonic Zonation Models are available for download on the Zenodo website: https://zenodo.org/records/18391170 with the following DOI: 10.5281/zenodo.18391170 (Mowbray et al., 2026). In the repository the following files are collected:

- *Sequenced_SZM_SE_France.ipynb* is the code compiled for data analysis, zone feature characterization and CLZL characterization.
- *SZM_virtual_map.html* shows the four SZM developed in this study in a user-friendly interactive map.
- *SZM.zip* contains a folder for each SZM which presents the datasets used to constrain each feature, grids, zone limits, zone feature values and CLZL values.
- *README.txt* describes the files comprised in SZM.zip, Sequenced_SZM_SE_France.ipynb and SZM_virtual_map.html

Author contributions

VM contributed to methodology development, feature and data choice, data analysis, code development, zone delineation, granting contribution weights for datasets and total feature difference levels for CLZL characterization, model deliberation, and writing. MM contributed with seismotectonic knowledge, methodology development, feature and data choice, data facilitation, data analysis, and writing. CS contributed with tectonic knowledge, methodology development, and writing. SB contributed with seismotectonic zonation knowledge, methodology development, feature and data choice, and writing. AL contributed with seismic and seismotectonic zonation knowledge, data choice, and writing. CB contributed with seismic hazard knowledge, seismic record knowledge, framework of previous SHA in France and in other countries, assessing seismic completeness periods, and writing.

Competing interests

The authors declare that they have no conflict of interest.

Acknowledgements

The authors would like to thank several researchers who have contributed by supplying data and methodological perspectives, namely Anne Paul, Louise Jeandet and Andrea Walpersdorf.

Financial support

This work has benefited from a government grant managed by the Agence nationale de la recherche as part of the France 2030 program, reference ANR-22-EXIR-0006. This work is also partially funded by the French Geological Survey (BRGM) of France, in the frame of the RGF-Alpes program, as well as by the French Ministry of Ecological Transition. Further support has been received from the ANR MADALPS project, bearing the reference code ANR-24-CE01-0721.

References

Autran, A., Blès J.-L., et Combes P., Cushing M., Dominique P., Durou Choux C., Gariel J.-C., Goula X., Mohammadioun B. & Terrier M. « Probabilistic seismic hazard assessment in France. Part One: seismotectonic zonation. » 11th European Conference on Earthquake Engineering, Balkema, Rotterdam., 1998.

https://doi.org/10.5194/egusphere-2026-623
Preprint. Discussion started: 5 March 2026

Baize, Stéphane, Edward Marc Cushing, Francis Lemeille, et Hervé Jomard. « Updated Seismotectonic Zoning Scheme of Metropolitan France, with Reference to Geologic and Seismotectonic Data ». Bulletin de La Société Géologique de France 184, nº 3, https://doi.org/10.2113/gssgfbull.184.3.225, 2013.

Baize, Stéphane, M. Cushing, Francis Lemeille, et al. « Inventaire des indices de rupture affectant le quaternaire. - En relation avec les grandes structures connues en Francs métropolitaine et dans les régions limitrophes ». Mém. Soc. géol. Fr., 2002, N°175, 142 pages. Mém. Soc. géol. Fr., 2002, N°175, 142 pages. Institut de Radioprotection et de Sûreté Nucléaire (IRSN). Fontenay aux Roses, 2002.

Basili, R., Valensise, G., Vannoli, P., Burrato, P., Fracassi, U., Mariano, S., Tiberti, M.M., Boschi, E. « The Database of Individual Seismogenic Sources (DISS), version 3: Summarizing 20 years of research on Italy's earthquake geology ». Tectonophysics 453, 20–43. https://doi.org/10.1016/j.tecto.2007.04.014, 2008.

BCSF-Rénass. « Instrumental Seismicity in Mainland France (1962-2021) ». Avec Université De Strasbourg, Marc Grunberg, Sophie Lambotte, et al. Prépublication, EOST UAR830, Université de Strasbourg, CNRS. Dataset: https://doi.org/10.25577/FV3F-SQ09, 2022.

Beauval, C., et O. Scotti. « Quantifying Sensitivities of PSHA for France to Earthquake Catalog Uncertainties, Truncation of Ground-Motion Variability, and Magnitude Limits ». Bulletin of the Seismological Society of America 94, nº 5, 1579-94. https://doi.org/10.1785/012003246, 2004.

Beauval, Céline, Oona Scotti, et Fabian Bonilla. « The Role of Seismicity Models in Probabilistic Seismic Hazard Estimation: Comparison of a Zoning and a Smoothing Approach ». Geophysical Journal International 165, nº 2, 584-95. https://doi.org/10.1111/j.1365-246X.2006.02945.x, 2006.

Beauval, Céline, Pierre-Yves Bard, et Laurentiu Danciu. « The Influence of Source- and Ground-Motion Model Choices on Probabilistic Seismic Hazard Levels at 6 Sites in France ». Bulletin of Earthquake Engineering 18, nº 10, 4551-80. https://doi.org/10.1007/s10518-020-00879-z, 2020.Bellahsen, N., F. Mouthereau, A. Boutoux, et al. « Collision Kinematics in the Western External Alps: Kinematics of the Alpine Collision ». Tectonics 33, nº 6, 1055-88, https://doi.org/10.1002/2013tc003453, 2014.

Bertrand, G, O Bellier, L Bollinger, et al. « NéoPal : Base de données nationale des déformations néotectoniques et des paléoséismes ». 7ème Colloque National AFPS 2007 - Ecole Centrale Paris, 2007.

Bienveignant, Dorian, Ahmed Nouibat, Christian Sue, et al. « Shaping the Crustal Structure of the SW-Alpine Foreland: Insights from 3D Geological Modeling ». Tectonophysics 889, 230471. https://doi.org/10.1016/j.tecto.2024.230471, 2024.

Boschetti, Louise, Malou Pelletier, Fréderic Mouthereau, et al. « Polyphase tectonic, thermal and burial history of the Vocontian basin revealed by U-Pb calcite dating ». Prépublication, Tectonic plate interactions, magma genesis, and lithosphere deformation at all scales/Structural geology and tectonics, paleoseismology, rock physics, experimental deformation/Structural geology, https://doi.org/10.5194/egusphere-2025-3332, 2025.

Braszus, Benedikt, Andreas Rietbrock, et Christian Haberland. « A 3D Velocity Model for the European Alps: New Insights Into the Crustal Structure ». Journal of Geophysical Research: Solid Earth 130, nº 10, e2025JB031877. https://doi.org/10.1029/2025JB031877, 2025.

Castaldo, R., L. D'Auria, S. Pepe, G. Solaro, V. De Novellis, et P. Tizzani. « The Impact of Crustal Rheology on Natural Seismicity: Campi Flegrei Caldera Case Study ». Geoscience Frontiers 10, nº 2, 453-66. https://doi.org/10.1016/j.gsf.2018.02.003, 2019.

https://doi.org/10.5194/egusphere-2026-623
Preprint. Discussion started: 5 March 2026

Chantraine, J., A. Autran, et C. Cavelier.« Carte géologique de la France (version numérique) à l'échelle du millionième », 2003.

Chartier, Thomas, Oona Scotti, Christophe Clément, Hervé Jomard, et Stéphane Baize. « Transposing an Active Fault Database into a Fault-Based Seismic Hazard Assessment for Nuclear Facilities – Part 2: Impact of Fault Parameter Uncertainties on a Site-Specific PSHA Exercise in the Upper Rhine Graben, Eastern France ». Natural Hazards and Earth System Sciences 17, nº 9, 1585-93. https://doi.org/10.5194/nhess-17-1585-2017, 2017.

Chiaraluce, L., M.R. Barchi, S. Carannante, et al. « The Role of Rheology, Crustal Structures and Lithology in the Seismicity Distribution of the Northern Apennines ». Tectonophysics 694, 280-91. https://doi.org/10.1016/j.tecto.2016.11.011, 2017.

Clément, C., O. Scotti, L. F. Bonilla, S. Baize, et C. Beauval. « Zoning versus faulting models in PSHA for moderate seismicity regions reliminary results for the tricastin nuclear site, France ». Bollettino Di Geofisica Teorica Ed Applicata, 45 (3), p.187-204, 2004.

Coppersmith, Kevin J., Robert R. Youngs, et Christian Sprecher. « Methodology and Main Results of Seismic Source Characterization for the PEGASOS Project, Switzerland ». Swiss Journal of Geosciences 102, nº 1, 91-105. https://doi.org/10.1007/s00015-009-1309-1, 2009.

Cornell, C. Allin. « Engineering Seismic Risk Analysis ». Bulletin of the Seismological Society of America 58, nº 5, 1583-606. https://doi.org/10.1785/bssa0580051583, 1968.

Danciu, Laurentiu, Shyam Nandan, Celso Reyes, et al. « ESHM20 - EFEHR Technical ReportThe 2020 Update of the European Seismic Hazard Model - ESHM20: Model Overview ». EFEHR European Facilities of Earthquake Hazard and Risk. https://doi.org/10.12686/A15, 2021.

Danciu, Laurentiu, Domenico Giardini, Graeme Weatherill, et al. « The 2020 European Seismic Hazard Model: Overview and Results ». Natural Hazards and Earth System Sciences 24, nº 9: 3049-73. https://doi.org/10.5194/nhess-24-3049-2024, 2024.

Delacou, Bastien, Christian Sue, Jean-Daniel Champagnac, et Martin Burkhard. « Origin of the Current Stress Field in the Western/Central Alps: Role of Gravitational Re-Equilibration Constrained by Numerical Modelling ». Geological Society, London, Special Publications 243, nº 1: 295-310. https://doi.org/10.1144/GSL.SP.2005.243.01.19, 2005.

Delacou, Bastien, Christian Sue, Jean-Daniel Champagnac, et Martin Burkhard. « Present-Day Geodynamics in the Bend of the Western and Central Alps as Constrained by Earthquake Analysis ». Geophysical Journal International 158, nº 2: 753-74. https://doi.org/10.1111/j.1365-246X.2004.02320.x, 2004.

Drouet, Stéphane, Gabriele Ameri, Kristell Le Dortz, Ramon Secanell, et Gloria Senfaute. « A Probabilistic Seismic Hazard Map for the Metropolitan France ». Bulletin of Earthquake Engineering 18, nº 5 (2020): 5. https://doi.org/10.1007/s10518-020-00790-7, 2020.

Fröhlich, C. « Triangle diagrams: ternary graphs to display similarity and diversity of earthquake focal mechanisms ». Physics of the Earth and Planetary Interiors, 75, 193–198, Elsewer Science Pubhshers B V, Amsterdam, 1992.

GeoMol Project Team. « GeoMol Geological Model 2019 – Mesozoic base ». Swiss Geological Survey / Swiss Federal Office of Topography. https://viewer.swissgeol.ch/, 2019.

https://doi.org/10.5194/egusphere-2026-623
Preprint. Discussion started: 5 March 2026

Grosset, Juliette, Stéphane Mazzotti, et Philippe Vernant. « Glacial-Isostatic-Adjustment Strain Rate–Stress Paradox in the Western Alps and Impact on Active Faults and Seismicity ». Solid Earth 14, nº 10: 1067-81. https://doi.org/10.5194/se-14-1067-2023, 2023.

Guéguen, Philippe, Gael Janex, Jérôme Nomade, et al. « Unprecedented Seismic Swarm in the Maurienne Valley (2017–2019) Observed by the SISmalp Alpine Seismic Network: Operational Monitoring and Management ». Comptes Rendus. Géoscience 353, nº S1: 517-34. https://doi.org/10.5802/crgeos.70, 2022.

Hanks, Thomas C., et Hiroo Kanamori. « A Moment Magnitude Scale ». Journal of Geophysical Research: Solid Earth 84, nº B5: 2348-50. https://doi.org/10.1029/JB084iB05p02348, 1979.

Hashemi, Kiana & Maharjan, Saroj & Ameri, Gabriele & Martin, Christophe & Benjelloun, Yacine & Poujol, Antoine & Baumont, David. « Comparison of seismic hazard models for South-Eastern France ». Proceedings, 18th World Conference on Earthquake Engineering (WCEE2024), 11 pages. Milan, Italy, 2024.

Hashemi, Kiana, Yacine Benjelloun, Saroj Maharjan, Antoine Poujol, David Baumont, et Christophe Martin. « A Comparison of Recent Seismic Hazard Models Covering Metropolitan France Developed at Different Scales ». Proceedings, 11ème Colloque National de l'AFPS. Guadeloupe, 12 pages. 2023.

Heidbach, Oliver, M. Rajabi, K. Reiter, et M. Ziegler. « World Stress Map 2016 ». GFZ Data Service. doi:10.5880/WSM.2016.002, 2016.

Heidbach, Oliver, Mark Tingay, Andreas Barth, John Reinecker, Daniel Kurfeß, et Birgit Müller. « Global Crustal Stress Pattern Based on the World Stress Map Database Release 2008 ». Tectonophysics 482, nºs 1-4: 3-15. https://doi.org/10.1016/j.tecto.2009.07.023, 2010.

Hengl, Tomislav, Leal Parente, Leandro, Krizan, Josip, and Bonannella, Carmelo. Continental Europe Digital Terrain Model. Distributed by OpenTopography. https://doi.org/10.5069/G99021ZF, 2022.

ISIDe Working Group avec Francesco Mariano Mele, Salvatore Mazza, Carlo Marcocci, et al. « Italian Seismological Instrumental and Parametric Database (ISIDe) ». Prépublication, Istituto Nazionale di Geofisica e Vulcanologia (INGV). https://doi.org/10.13127/ISIDE, 2007.

Jeandet Louise, Mazzotti Stéphane and Jomard Hervé. « Present-day tectonics in mainland France and nearby regions based on GNSS and earthquake focal mechanism data », Submitted.

Jenatton, Liliane, Robert Guiguet, François Thouvenot, et Nicolas Daix. « The 16,000-event 2003–2004 Earthquake Swarm in Ubaye (French Alps) ». Journal of Geophysical Research: Solid Earth 112, nº B11: 2006JB004878. https://doi.org/10.1029/2006JB004878, 2007.

Jomard, Hervé, Edward Marc Cushing, Luigi Palumbo, Stéphane Baize, Claire David, et Thomas Chartier. « Transposing an Active Fault Database into a Seismic Hazard Fault Model for Nuclear Facilities – Part 1: Building a Database of Potentially Active Faults (BDFA) for Metropolitan France ». Natural Hazards and Earth System Sciences 17, nº 9: 9. https://doi.org/10.5194/nhess-17-1573-2017, 2017.

Kostrov, V. V. « Seismic moment and energy of earthquakes, and seismic flow of rock. » Izv. Acad. Sci. USSR Phys. Solid Earth Engl. Transl., 1, 23–44, 1974.

Lammers, Steffi, Graeme Weatherill, Gottfried Grünthal, et Fabrice Cotton. « EMEC-2021 - The European-Mediterranean Earthquake Catalogue – Version 2021 ». GFZ German Research Center for Geosciences. https://doi.org/10.5880/GFZ.EMEC.2021.001, 2023.

https://doi.org/10.5194/egusphere-2026-623
Preprint. Discussion started: 5 March 2026

Langlais, Mickael, Gael Janex, Philippe Guéguen, et al. « The Catalogue of 1987–2023 Earthquakes in the Western (French) Alps North of 43.5°N ». Scientific Data 11, nº 1: 1290. https://doi.org/10.1038/s41597-024-04133-y, 2024.

Lantmäteriet. « EPOS Horizontal Strain Rates ». The Swedish mapping, Cadastral and land Registration authority. [Dataset] https://doi.org/10.23701/SR, 2023.

Larroque, Christophe, Stéphane Baize, Julie Albaric, et al. « Seismotectonics of Southeast France: From the Jura Mountains to Corsica ». Comptes Rendus. Géoscience 353, nº S1: 105-51. https://doi.org/10.5802/crgeos.69, 2021.

Le Dortz, Kristell Le, Philippe Combes, et David Carbon. « An Alternative Seismotectonic Zonation for Probabilistic and Deterministic Seismic Hazard Assessment for Metropolitan France ». 10ème Colloque National AFPS 2019. Strasbourg, 2019.

Le Pichon, Xavier, et Claude Rangin. « Geodynamics of the France Southeast Basin: Importance of Gravity Tectonics ». Bulletin de La Société Géologique de France 181, nº 6: 476-476. https://doi.org/10.2113/gssgfbull.181.6.476, 2010.

Lu, Yang, Laurent Stehly, Anne Paul, et AlpArray Working Group. « High-Resolution Surface Wave Tomography of the European Crust and Uppermost Mantle from Ambient Seismic Noise ». Geophysical Journal International 214, nº 2: 1136-50. https://doi.org/10.1093/gji/ggy188, 2018.

Malavieille, Jacques. « Late Orogenic Extension in Mountain Belts: Insights from the Basin and Range and the Late Paleozoic Variscan Belt ». Tectonics 12, nº 5: 1115-30. https://doi.org/10.1029/93TC01129, 1993.

Manchuel, K., P. Traversa, D. Baumont, M. Cara, E. Nayman, et C. Durouchoux. « The French Seismic CATalogue (FCAT-17) ». Bulletin of Earthquake Engineering 16, nº 6: 6. https://doi.org/10.1007/s10518-017-0236-1, 2018.

Martin, Christophe, P. Combes, R. Secanell, et al. « Révision du zonage sismique de la France. Étude probabiliste ». GTR/MATE/0701-150, MATE, Paris (in French). Édition, 2002.

Martin, Christophe, Gabriele Ameri, David Baumont, et al. « Probabilistic Seismic Hazard Assessment for South-Eastern France ». Bulletin of Earthquake Engineering 16, nº 6: 6. https://doi.org/10.1007/s10518-017-0249-9, 2018.

Masson, Christine, Stephane Mazzotti, Philippe Vernant, et Erik Doerflinger. « Extracting Small Deformation beyond Individual Station Precision from Dense Global Navigation Satellite System (GNSS) Networks in France and Western Europe ». Solid Earth 10, nº 6: 1905-20. https://doi.org/10.5194/se-10-1905-2019, 2019.

Mathey, Marguerite, Andrea Walpersdorf, Christian Sue, Stéphane Baize, et A. Deprez. « Seismogenic Potential of the High Durance Fault Constrained by 20 Yr of GNSS Measurements in the Western European Alps ». Geophysical Journal International 222, nº 3: 2136-46. https://doi.org/10.1093/gji/ggaa292, 2020.

Mathey, Marguerite, Sue, C., Pagani, C., Baize, S., Walpersdorf, A., Bodin, T., Husson, L., Hannouz, E., Potin, B. « Present-day geodynamics of the Western Alps: new insights from earthquake mechanisms ». Solid Earth 12, 1661–1681. https://doi.org/10.5194/se-12-1661-2021, 2021.

Mathey, Marguerite, M.-P. Doin, P. André, A. Walpersdorf, S. Baize, et C. Sue. « Spatial Heterogeneity of Uplift Pattern in the Western European Alps Revealed by InSAR Time-Series Analysis ». Geophysical Research Letters 49, nº 1: 1. https://doi.org/10.1029/2021GL095744, 2022.

https://doi.org/10.5194/egusphere-2026-623
Preprint. Discussion started: 5 March 2026

Mazzotti, Stephane, Clémence Aubagnac, Laurent Bollinger, et al. « FMHex20: An Earthquake Focal Mechanism Database for Seismotectonic Analyses in Metropolitan France and Bordering Regions ». BSGF - Earth Sciences Bulletin 192: 10. https://doi.org/10.1051/bsgf/2020049, 2021.

McGuire, Robin K. « FORTRAN computer program for seismic risk analysis ». Open-File Report. US Geological Survey. https://doi.org/10.3133/ofr7667, 1976.

Mohn, G., G. Manatschal, M. Beltrando, E. Masini, et N. Kusznir. « Necking of Continental Crust in Magma-poor Rifted Margins: Evidence from the Fossil Alpine Tethys Margins ». Tectonics 31, nº 1: 2011TC002961. https://doi.org/10.1029/2011TC002961, 2012.

Mowbray, Victoria, Sue, C., Baize, S., Beauval, C., Mathey, M., Lemoine, A., Walpersdorf, A., Granier, E. « South East France Potentially Active Faults: A database for seismic hazard assessment ». Preprint. Earth Syst. Sci. Data Discuss., 1–30. https://doi.org/10.5194/essd-2025-601, 2025.

Mowbray, Victoria, Mathey, M., Sue, C., Baize, S., Lemoine, A., Beauval, C. « Sequenced seismotectonic zonation models for South-East France ». Zenodo Database [dataset]. https://doi.org/10.5281/zenodo.18391170, 2026.

Nouibat, A, L Stehly, A Paul, et al. « Lithospheric Transdimensional Ambient-Noise Tomography of W-Europe: Implications for Crustal-Scale Geometry of the W-Alps ». Geophysical Journal International 229, nº 2: 862-79. https://doi.org/10.1093/gji/ggab520, 2022.

Nouibat, Ahmed. « Eucrust_transD-ANT ». Data Terra, Database [dataset]. https://doi.org/10.57932/AD29E767-15A6-4DD1-A2D1-B7AFE6E45F73, 2024.

Petit, Carole, Louis de Barros, Guillaume Duclaux, and Yves Mazabraud. 2019. « Why Are There No Earthquakes in the Intracratonic Paris Basin? Insights from Flexural Models » *Geosciences* 9, no. 12: 502. https://doi.org/10.3390/geosciences9120502, 2019.

Piña-Valdés, Jesús, Anne Socquet, Céline Beauval, Marie-Pierre Doin, Nicola D'Agostino, et Zheng-Kang Shen. « 3D GNSS Velocity Field Sheds Light on the Deformation Mechanisms in Europe: Effects of the Vertical Crustal Motion on the Distribution of Seismicity ». Journal of Geophysical Research: Solid Earth 127, nº 6: e2021JB023451. https://doi.org/10.1029/2021JB023451, 2022.

Rovida, Andrea, Andrea Antonucci, et Mario Locati. « The European Preinstrumental Earthquake Catalogue EPICA, the 1000–1899 Catalogue for the European Seismic Hazard Model 2020 ». Earth System Science Data 14, nº 12: 5213-31. https://doi.org/10.5194/essd-14-5213-2022, 2022.

Secanell, R., D. Bertil, C. Martin, et al. « Probabilistic Seismic Hazard Assessment of the Pyrenean Region ». Journal of Seismology 12, nº 3: 3. https://doi.org/10.1007/s10950-008-9094-2, 2008.

Serpelloni, Enrico, Adriano Cavaliere, Leonardo Martelli, et al. « Surface Velocities and Strain-Rates in the Euro-Mediterranean Region From Massive GPS Data Processing ». Frontiers in Earth Science 10: 907897. https://doi.org/10.3389/feart.2022.907897, 2022.

Spooner, Cameron, Magdalena Scheck-Wenderoth, Hans-Jürgen Götze, Jörg Ebbing, György Hetényi, et the AlpArray Working Group. « Density Distribution across the Alpine Lithosphere Constrained by 3-D Gravity Modelling and Relation to Seismicity and Deformation ». Solid Earth 10, nº 6: 2073-88. https://doi.org/10.5194/se-10-2073-2019, 2019.

https://doi.org/10.5194/egusphere-2026-623
Preprint. Discussion started: 5 March 2026

Sternai, Pietro, Christian Sue, Laurent Husson, et al. « Present-Day Uplift of the European Alps: Evaluating Mechanisms and Models of Their Relative Contributions ». Earth-Science Reviews 190: 589-604. https://doi.org/10.1016/j.earscirev.2019.01.005, 2019.

Sue, Christian, Bastien Delacou, Jean-Daniel Champagnac, Cecile Allanic, et Martin Burkhard. « Aseismic Deformation in the Alps: GPS vs. Seismic Strain Quantification ». Terra Nova 19, nº 3: 182-88. https://doi.org/10.1111/j.1365-3121.2007.00732.x, 2007a.

Sue, Christian, Bastien Delacou, Jean-Daniel Champagnac, Cécile Allanic, Pierre Tricart, et Martin Burkhard. « Extensional Neotectonics around the Bend of the Western/Central Alps: An Overview ». International Journal of Earth Sciences 96, nº 6: 1101-29. https://doi.org/10.1007/s00531-007-0181-3, 2007b.

Sue, Christian, François Thouvenot, Julien Fréchet, et Pierre Tricart. « Widespread Extension in the Core of the Western Alps Revealed by Earthquake Analysis ». Journal of Geophysical Research: Solid Earth 104, nº B11: 25611-22. https://doi.org/10.1029/1999JB900249, 1999.

Terrier, M., J.L. Blès, P. Godefroy†, P. Dominique, M. Bour, et C. Martin. « Zonation of Metropolitan France for the Application of Earthquake-Resistant Building Regulations to Critical Facilities Part 1: Seismotectonic Zonation ». Journal of Seismology 4, nº 3: 215-30. https://doi.org/10.1023/A:1009896630858, 2000.

Valla, Pierre G., Pietro Sternai, et Matthew Fox. « How Climate, Uplift and Erosion Shaped the Alpine Topography ». Elements 17, nº 1: 41-46. https://doi.org/10.2138/gselements.17.1.41, 2021.

Walpersdorf, A., L. Pinget, P. Vernant, C. Sue, A. Deprez, et the RENAG team. « Does Long-Term GPS in the Western Alps Finally Confirm Earthquake Mechanisms? » Tectonics 37, nº 10: 3721-37. https://doi.org/10.1029/2018TC005054, 2018.

Walpersdorf, A., C. Sue, S. Baize, et al. « Coherence between Geodetic and Seismic Deformation in a Context of Slow Tectonic Activity (SW Alps, France) ». Journal of Geodynamics 85: 58-65. https://doi.org/10.1016/j.jog.2015.02.001, 2015.

Woessner, Jochen, Danciu Laurentiu, Domenico Giardini, et al. « The 2013 European Seismic Hazard Model: Key Components and Results ». Bulletin of Earthquake Engineering 13, nº 12: 3553-96. https://doi.org/10.1007/s10518-015-9795-1, 2015.

Zielke, Olaf, Danijel Schorlemmer, Sigurjon Jónsson, et Paul Martin Mai. « Magnitude-Dependent Transient Increase of Seismogenic Depth ». Seismological Research Letters 91, nº 4: 2182-91. https://doi.org/10.1785/0220190392, 2020.